Mechanisms of goethite dissolution in the presence of desferrioxamine B and Suwannee River fulvic acid at pH 6.5

Angela G. Stewart[a, b], Karen A. Hudson-Edwards[a] and William E. Dubbin[b*]

[a] Department of Earth and Planetary Sciences, Birkbeck, University of London, Malet St., London WC1E 7X, UK

[b] Department of Earth Science, The Natural History Museum, Cromwell Road, London SW7 5BD, UK. *Corresponding author. Email: b.dubbin@nhm.ac.uk

tel: +44 (0)20-7942-5616

fax: +44 (0)20-7942-5537

Abstract

Siderophores are Fe^{3+} specific low MW chelating ligands secreted by micro-organisms in response to Fe stress. Low MW organic acids such as oxalate have been shown to enhance siderophore mediated dissolution of Fe^{3+} oxides. However, the effect of fulvic acid presence on siderophore function remains unknown. We used batch dissolution experiments to investigate Fe release from goethite in the goethite-fulvic acid-desferrioxamine B (goethite-SRFA-DFOB) ternary system. Experiments were conducted at pH 6.5 while varying reagent addition sequence. FTIR and UV-Vis spectroscopy were employed to characterise the Fe-DFOB, Fe-SRFA and DFOB–SRFA complexes. Iron released from goethite in the presence of SRFA alone was below detection limit. In the presence of both SRFA and DFOB, dissolved Fe increased with reaction time, presence of the DFOB-SRFA complex, and where SRFA was introduced prior to DFOB. FTIR data show that in the ternary system, Fe^{3+} is complexed primarily to oxygen of the DFOB hydroxamate group, whilst the carboxylate C=O of SRFA forms an electrostatic association with the terminal NH_3^+ of DFOB. We propose that SRFA sorbed to goethite lowers the net positive charge of the oxide surface, thus facilitating adsorption of cationic DFOB and subsequent Fe^{3+} chelation and release. Furthermore, the sorbed SRFA weakens Fe-O bonds at the goethite surface, increasing the population of kinetically labile Fe. This work demonstrates the positive, though indirect role of SRFA in increasing the bioavailability of Fe^{3+}.

Keywords: siderophore, goethite, dissolution, Suwannee River fulvic acid, desferrioxamine

45 # 1. INTRODUCTION

46

47 In oxic soils and sediments, Fe availability is limited by the low solubility of Fe
48 oxides at circumneutral pH (Raymond and Dertz, 2004). To obtain Fe from these sparingly
49 soluble phases, low MW Fe^{3+}-chelating ligands known as siderophores are released by plants
50 and micro-organisms (Haselwandter, 2008). For example, twice as much Fe is solubilised
51 from goethite in the presence of 126 μM desferrioxamine B (DFOB), a trihydroxamate
52 siderophore, than in the presence of 100 mM HCl at pH 3 over a 28-day reaction (Watteau
53 and Berthelin, 1994). Furthermore, at hydroxamate siderophore concentrations typical of
54 soils (i.e. 10^{-7} – 10^{-8} M; Powell et al., 1980), goethite solubility increases over a wide pH
55 range (Kraemer, 2004), where the dissolution of goethite at pH > 4 is described as ligand-
56 controlled (Holmén and Casey, 1996; Reichard et al., 2007a).

57 Iron(III) is coordinated to the hydroxamate groups of DFOB (Fig. 1) with Fe oxide
58 dissolution influenced by siderophore concentration (Liermann et al., 2000), solution pH
59 (Cervini-Silva, 2008) and temperature (Cocozza et al., 2002). As revealed by single-crystal
60 X-ray diffraction, the chelate molecule consists of two closed loops and a free chain
61 containing a protonated amine (Dhungana et al, 2001). The six hydroxamate oxygen atoms
62 coordinate Fe^{3+} and form a distorted octahedral geometry around the metallic centre (Cozar et
63 al., 2006; Domagal-Goldman et al., 2009) (Fig. 1b). As a consequence of this complexation,
64 the hydroxamate (oxime) protons are lost and the goethite hydroxyl or water groups
65 coordinating Fe^{3+} are displaced.

66 Iron release from goethite may be enhanced by the presence of low MW organic
67 acids. For example, goethite dissolution by 5×10^{-5} M oxalate, malonate or succinate at pH 6
68 yielded 10^{-11} M Fe following 400 h reaction (Reichard et al., 2007a) while the presence of
69 citrate produced 10^{-7} M Fe and fumarate yielded undetectable levels of dissolved Fe. When

DFOB was added to those systems containing both goethite and low MW organic acids, greater amounts of Fe were released than in DFOB-only goethite systems. For example, soluble Fe concentrations increased from 10^{-11} M to 10^{-5} M when 5.0×10^{-5} M DFOB was added to a goethite suspension along with equimolar concentrations of the organic ligands listed above, except for citrate, for which soluble Fe increased only marginally, from 10^{-7} M to 10^{-6} M.

Fulvic acid (FA) (Fig. 2), the acid soluble component of humic substances are, along with hydrous Fe oxides and siderophores, ubiquitous in soils and sediments (Stevenson, 1985). Fulvic acid sorbs strongly to goethite surfaces at pH values below the point of zero charge for goethite (i.e. < 9.2, Filius et al., 2000). This adsorption involves the formation of inner-sphere complexes via ligand exchange between the oxygen of FA carboxylate groups and the surface oxygen atoms coordinated to Fe at the goethite surface (Filius et al., 2003). Fourier transform infrared (FTIR) spectroscopy confirms the formation of this inner-sphere Fe-fulvate complex by virtue of a shift in the asymmetric carboxylate stretch vibration at pH 5 (Fu and Quan, 2006). Humic compounds obtained from various natural environments also complex strongly, and reversibly, with mononuclear Fe, exhibiting stability constants of $10^{21.0}$ to $10^{21.4}$ for Fe-humic complexes isolated from a river plume (Muller and Batchelli, 2011), with lower stability constants (i.e. $K = 10^{11.5}$ to $10^{14.0}$) observed for Fe-FA complexes obtained from soil (Pandeya, 1993).

Although the effects of low MW acids such as oxalate and citrate on DFOB mediated dissolution of goethite have been examined previously (Reichard et al., 2007a,b), the influence of the higher MW fulvic acid has not yet been explored despite the ubiquity of this humic material in soils and sediments. In this paper we report, for the first time, the results of batch experiments examining the dissolution of goethite in the presence of both Suwannee River fulvic acid (SRFA) and DFOB. The effects of SRFA presence and reagent addition

95 sequence were investigated at pH 6.5 to elucidate dissolution mechanisms. The aims of the
96 study were to: (i) determine the effect of SRFA presence on goethite dissolution by DFOB;
97 (ii) develop a mechanistic model of how SRFA influences DFOB function; (iii) characterise
98 possible aqueous Fe-DFOB and Fe-SRFA complexes formed; (iv) propose an overall
99 dissolution mechanism for the goethite-DFOB-SRFA system.
100
101 ## 2. MATERIALS AND METHODS
102
103 ### 2.1. Goethite synthesis and characterisation
104
105 Goethite was synthesised following the method of Schwertmann and Cornell (1991).
106 Briefly, 180 mL of 5 M KOH (Fisher Chemicals, SLR) was rapidly added to 100 mL of 1 M
107 $Fe(NO_3)_3.9H_2O$ (BDH, AnalaR) in a 2 L plastic beaker with constant stirring for 10 min. The
108 suspension was brought to 2 L with ultrapure water (18 MΩ-cm, Milli-Q Millipore) and
109 transferred to five 500 mL amber wide-mouth Nalgene HDPE screw top bottles then aged for
110 24 h at 70 °C (Dubbin and Ander, 2003). The precipitate was washed with ultrapure water
111 through a Büchner funnel into a Büchner flask using Whatman no. 40 filter paper, which was
112 replaced after every 250 mL of suspension to prevent clogging. The precipitate was then
113 allowed to air-dry at 21 °C.
114 The hydroxy Fe precipitates were confirmed as goethite (α-FeOOH) by powder X-ray
115 diffraction (XRD) analyses on an Enraf-Nonius PSD 120, equipped with an INEL 120°
116 curved position sensitive detector utilising Cu $K\alpha_1$ radiation (45 kV and 45 mV) at 25 °C. N_2
117 multipoint BET surface area measurements were carried out using a Micrometrics Gemini III
118 2375 instrument. Samples were allowed to de-gas with N_2 at 100 °C for 24 h prior to surface

119 area determination. A kaolinite standard (15.9 $\pm$ 0.8 m^2/g) was analysed alongside the
120 goethite samples to monitor accuracy.
121
122 ## 2.2. Batch dissolution experiments
123
124 Stock solutions of: (i) DFOB obtained as the mesylate salt
125 [$(C_{25}H_{46}N_5O_8NH_3^+(CH_3SO_3^-)$, MW 656 g mol^{-1}] (Sigma-Aldrich); (ii) SRFA purchased from
126 the International Humic Substance Society [IHSS, Sample 1S101F, MW 1360 g mol^{-1} (Chin
127 et al., 1994)]; and (iii) synthetic goethite (α-FeOOH) were prepared in a combined
128 buffer/electrolyte (MOPS/$NaNO_3$) solution for subsequent use in the batch dissolution
129 experiments. Both DFOB and SRFA were used as received to prepare a 500 μM stock
130 solution of DFOB (0.823 g DFOB dissolved in 250 mL MOPS/$NaNO_3$ solution) and a 65 mg
131 C L^{-1} stock solution of SRFA (0.0624 g SRFA dissolved in 500 mL MOPS/$NaNO_3$ solution).
132 The goethite stock suspension was prepared to a concentration of 1256 mg L^{-1} (3.14 g
133 goethite in 2500 mL MOPS/$NaNO_3$ solution). The combined MOPS/$NaNO_3$ solution
134 consisted of 1 mM 3-(N-morpholino) propanesulfonic acid (MOPS), a non-complexing
135 buffer (Electran VWR BDH PRO LAB molecular biology grade; pH range 6.5 – 7.9; pK_a
136 7.2), and 10 mM $NaNO_3$ (BDH AnalaR). The pH of the MOPS/$NaNO_3$ solution was
137 increased from pH 4.5 to 6.5 with the drop-wise addition of 0.1 M NaOH (BDH ARISTAR),
138 continuously monitored with a HANNA Instruments pH meter calibrated at two points (pH
139 4.01 and 7.01). The pH of the goethite suspensions, and DFOB and SRFA solutions, were
140 within the required range therefore no adjustment was required. Solutions and suspensions
141 were stored in amber HDPE wide-mouth screw top bottles to protect from photo-induced
142 reactions and stored at 4 °C to restrict microbial growth. All glassware and plasticware was

143 washed thoroughly with phosphate-free detergent (Decon 90) then rinsed several times with
144 ultra pure water.
145 Fig. 3 shows the reagents, addition sequences, and reaction times for each of the ten
146 batch experiments. For batch experiments 1 through 8 (carried out in duplicate) 90 mL of
147 goethite suspension was dispensed into each of eight 250 mL amber HDPE bottles. One of
148 these eight bottles contained goethite alone (system 8), while a further two bottles without
149 goethite served as procedural blanks to check for adsorption of DFOB (system 9) and SRFA
150 (system 10) onto container walls. Subsequently, 9 mL of DFOB stock solution or 30 mL of
151 SRFA stock solution were added to the bottles (with the exception of systems 3 and 5) as
152 indicated in Fig. 3. The DFOB-SRFA complex was equilibrated for 30 minutes before
153 addition to the goethite suspension (system 6). All batches were brought to a total volume of
154 129 mL with MOPS/$NaNO_3$ and left to equilibrate for 24 h at 25 °C on an orbital shaker
155 (Orbital Incubator SI50) at 100 rpm.
156 Following the initial 24 h contact, further reagents were added as indicated in Fig. 3,
157 brought to final volumes of 168 mL, then placed on the orbital shaker for the duration of the
158 reaction. In systems 3 and 5 we added DFOB and SRFA 4 h before the subsequent addition
159 of, respectively, SRFA and DFOB, to more fully explore the effect of DFOB and SRFA
160 addition sequence. A 4 hour reaction time was chosen because this duration had been
161 reported as the optimal reaction period to achieve ligand adsorption without significant
162 dissolution (Cocozza et al., 2002). The concentration of DFOB, where present, was 270 μM
163 in all batch experiments. The pH of the suspensions in the 250 mL bottles was measured
164 before and after the initial 24 h period, and at the end of the 330 h reaction. In all cases the
165 pH was maintained at 6.5 and did not need further adjusting. Maintaining pH at 6.5 ensured
166 that proton promoted dissolution was negligible. Changes in H^+ activity may also influence
167 ligand-controlled goethite dissolution by modifying the concentrations and speciation of

168 adsorbed ligands (Reichard et al., 2007b). Subsamples of the suspensions were obtained at
169 intervals throughout the 330 h reaction, then filtered through 25 mm cellulose acetate filters
170 (pore size 0.2 μm) followed by filtration through 25 mm nitrocellulose membrane filters
171 (pore size 0.025 μm) into clear polythene screw cap tubes.
172
173 ## 2.3. Analysis of supernatant solutions
174
175 Five mL portions of the filtrates were acidified with 100 μL 70% HNO_3 (Fisher
176 Scientific) to prevent precipitation of Fe hydroxide then stored at 4 °C. These solutions were
177 analysed for Fe using inductively coupled plasma atomic emission spectroscopy (ICP-AES)
178 analysis (VARIAN VISTA PRO Program ICP Expert version 4.1.0; emission line 259.94 nm;
179 detection limit 89 nmol Fe L^{-1}). Aqueous SRFA and DFOB were quantified by UV-Vis
180 spectroscopy (section 2.5). Total aqueous organic carbon (TOC) was determined by wet
181 combustion with a Shimadzu 5000 TOC analyser after acidification of the filtrate with 10 μL
182 concentrated HCl (BDH ARISTAR). To test the reliability of SRFA quantification by UV-
183 Vis spectroscopy (Gan et al., 2007; Ghabbour and Davies, 2009), aqueous SRFA
184 concentrations were also determined by TOC analysis, subtracting from the total organic C,
185 that C assigned to DFOB as determined by chelometric UV-Vis spectroscopy analysis
186 (section 2.5). Statistical significance among aqueous Fe, DFOB and SRFA concentrations for
187 all batches was determined by applying the unpaired two-tailed Student's *t*-test with a level of
188 significance of $p = 0.05$. The precipitate retained on each membrane filter following filtration
189 was air-dried at room temperature, placed in an air tight container and preserved for
190 subsequent observation by scanning electron microscopy (SEM), atomic force microscopy
191 (AFM) and FTIR analysis, described below.
192

2.4. FTIR spectroscopy

Synthetic goethite, untreated SRFA and DFOB, and aqueous complexes of SRFA and DFOB prepared in several mole ratios (2:1 Fe^{3+}-DFOB, 5:1 Fe^{3+}-SRFA, 1:1 DFOB-SRFA, and 5:1:1 Fe^{3+}-DFOB-SRFA) were analysed by FTIR. Iron(III) chloride hexahydrate ($FeCl_3.6H_2O$) was used to prepare the Fe^{3+}-complexes. Solid samples for FTIR analysis were obtained from the acidified aqueous complexes by concentrating the solutes through freeze drying (Triad LABCONCO with a JAVAC JL-10 high vacuum pump) to minimise infrared absorption by water and improve peak/band resolution. All samples, including the air-dried residues from filtration, were prepared for FTIR analysis using the KBr pellet technique (Prasad et al., 2006), mixing ~1 mg of sample with 100–200 mg spectroscopy grade KBr (Merck, IR spectroscopy, Uvasol®). When not in use, the pellets were stored in a desiccator to minimise uptake of water. All FTIR data were collected over 200–4000 cm^{-1} on a Perkin Elmer Spectrum One FTIR spectrometer with dedicated spectrum handling software (version 5.0.1). The spectra have a resolution of 4 cm^{-1} and are the aggregate of 128 scans.

2.5. SRFA and DFOB quantification

Filtrate SRFA was quantified by first obtaining a UV-Vis scan (220-900 nm) of a standard aqueous SRFA solution (31.2 mg SRFA L^{-1}) to obtain the λ_{max} (254 nm). A series of aqueous SRFA solutions of varying concentration were then prepared to construct the calibration curve. Aqueous SRFA from each batch dissolution experiment was then determined by placing 1 mL filtrate in micro cuvettes of 10 mm path length and measuring UV absorption at 254 nm (Qu et al., 2003; Tatár et al, 2004). Absorbance readings were obtained on a Shimadzu UV-1800 spectrophotometer fitted with tungsten iodine (visible) and

deuterium (UV) lamps. An aliquot of acidified MOPS/$NaNO_3$ was used to base correct the UV-Vis spectrophotometer before analysis of batch solutions.

Siderophore concentrations in the filtrates from the adsorption experiments were determined following the chelometric method (Cocozza et al., 2002; Cheah et al., 2003). Spectrophotometric measurements of the Fe-DFOB complex were obtained at 467 nm within 1 h after filtration. Filtrates and standards were acidified to pH 1.5 to 1.7 with 8 µL 70% $HClO_4$ (BDH ARISTAR). We then added 170 µL of 15 mM $Fe(ClO_4)_3$ to each filtrate sample to give an Fe concentration in excess of that needed to complex all DFOB. Analogous siderophore-free blank solutions containing only MOPS buffer, background electrolyte and added Fe were likewise acidified to pH 1.5 to 1.7. Subtraction of absorbance for the blank solution from that for the sample filtrates yielded the net absorbance, which we attribute to siderophore not adsorbed. The DFOB surface excess (µmol g^{-1}) was determined by dividing the siderophore concentration loss (i.e. 270 µM minus DFOB concentration in the filtrate) by the goethite concentration. DFOB quantification in system 9 (i.e. DFOB without goethite) served as a validation step to account for any DFOB sorbed to container walls and filters.

UV-Vis spectra were obtained for DFOB, $Fe(ClO_4)_3$, SRFA, Fe^{3+}-DFOB, Fe^{3+}-SRFA, DFOB-SRFA and Fe-DFOB-SRFA standard solutions prepared in a MOPS/$NaNO_3$ matrix and compared to the spectra of the batch filtrate solutions. Furthermore, the spectrum of a MOPS/$NaNO_3$ solution was compared to that of deionized water to ensure that MOPS/$NaNO_3$ peaks did not overlap those from Fe-DFOB.

2.6. SEM and AFM imaging

Goethite morphology was determined before and after reaction with SRFA and DFOB. Powdered goethite samples were fixed to Al stubs then coated with Au-Pd prior to

243 analysis on a Zeiss Gemini Ultra Plus SEM operating at 5.0 kV and a spot size of 20.00 μm
244 over a range of magnifications to observe gross particle morphology. AFM was used to
245 determine the surface relief of the goethite crystals. The analysis was conducted using an
246 Asylum MFP-3D-SA (Santa Barbara, USA) instrument in AC mode. The prepared film
247 samples (1 cm^2) were placed on glass slides and scanned in air over a 10 × 10 μm^2 area using
248 an Olympus AC240TS tip (spring constant 2 N m^{-1}). Surface roughness, amplitude and height
249 channels were monitored and analysed using IGOR PRO software.
250
251 # 3. RESULTS
252
253 ## 3.1. Characterisation of goethite
254
255 The addition of 5 M KOH to 1 M $Fe(NO_3)_3.9H_2O$ produced a brownish-yellow
256 precipitate of Munsell colour 10YR 6/8. The precipitates were confirmed as goethite (α-
257 FeOOH) by comparing their powder X-ray diffraction patterns with those reported in the
258 International Centre for Diffraction Data® Files (ICDD Files 1081-464). All the peaks
259 produced by the precipitates related to the structure of goethite; the absence of extraneous
260 peaks indicated that no other phases were present at detectable levels.
261 Analysis of goethite morphology by SEM showed the crystals to be lathed shaped as
262 observed previously (Cornell et al., 1974; Kosmulski et al., 2004). The fractured appearance
263 of some crystals we attribute to desiccation and water loss under high vacuum. The height of
264 the crystals obtained through AFM analysis was ~ 60 nm, while the N_2-BET surface area was
265 43 $m^2 g^{-1}$, slightly greater than that reported elsewhere (e.g. 35±3 $m^2 g^{-1}$; Kraemer et al.,
266 1999; 38 $m^2 g^{-1}$; Carrasco et al., 2007). Sorbed SRFA imparts surface roughness to goethite
267 and disrupts its characteristic lath-shaped morphology.

3.2. Goethite dissolution

Iron release kinetics for goethite dissolution in the presence of DFOB and / or SRFA at 270 μM initial siderophore concentration are shown in Fig. 4. Soluble Fe is detected only for those systems containing both goethite and DFOB (i.e. systems 1 – 6). At reaction times > 50 h Fe release broadly followed zero-order kinetics, with Fe concentration depending linearly on time (Table 1). This linearity is commonly observed for far from equilibrium dissolution reactions (Sposito, 1994; Lasaga, 1998), where the slope of the regression line equation (Table 1, column 2) is equal to the zero-order rate coefficient. Generally, goethite suspensions containing both DFOB and SRFA (e.g. systems 4, 5, 6) show increased slopes of the linear fits and greater soluble Fe than those containing only DFOB (i.e. system 1). This observation corroborates the complementary work of Reichard et al. (2007a) on two-ligand systems, who reported increased goethite dissolution at pH 6 in the presence of 50 μM DFOB alongside 50 μM oxalate, malonate, succinate or fumarate. These workers observed that in the presence of 50 μM DFOB alone, goethite dissolution yielded ~ 5 μM Fe, but this increased to nearly 10 μM Fe with the addition of the above low molecular weight organic ligands. Furthermore, in our study, addition of SRFA prior to DFOB (i.e. systems 4 and 5) yielded greater slopes than for those systems where DFOB was introduced prior to SRFA (i.e. systems 2 and 3). Introduction of the DFOB-SRFA complex to the goethite suspension (system 6) gave rise to the greatest Fe release.

In dissolution reactions under far from equilibrium conditions, the zero-order rate coefficient is generally considered to be proportional to either: (i) the specific surface area or (ii) the mass of the dissolving solid (Lasaga, 1998). However, as the normalisation of dissolution rates with respect to surface area is not straightforward (Brantley and Chen,

293 1995), we express the dissolution rates with respect to mass of the goethite. Mass normalised
294 rate coefficients (μmol g^{-1} h^{-1}) were therefore derived as the slope of the linear fit divided by
295 the goethite mass, and these coefficients are presented in column 3 of Table 1. The mass-
296 normalised dissolution rate coefficients are greatest for those systems containing SRFA,
297 particularly where this humic material was introduced prior to DFOB. Interestingly, the
298 simultaneous introduction of DFOB and SRFA as the DFOB-SRFA complex (system 6)
299 yielded the greatest rate coefficient of all systems.

300 The mass-normalised dissolution rate reported by Cocozza et al. (2002) for the
301 dissolution of goethite by DFOB at 25 °C (i.e. 0.135 μmol g^{-1} h^{-1}) is approximately one-half
302 that reported here (i.e. 0.257 μmol g^{-1} h^{-1}). Some of this difference may arise from the slightly
303 higher concentration of DFOB used in this study (i.e. 270 μM vs. 240 μM). However, most of
304 this difference in dissolution rate can be attributed to variation in the nature of the goethite
305 sample. Cornell and Schwertmann (2003), for example, cite the influence of goethite
306 morphology and crystallinity as important determinants of dissolution rate. The goethite used
307 in this study was prepared using a method broadly similar to that adopted by Cocozza et al.
308 (2002), with the exception that these earlier workers incorporated a longer aging period
309 yielding a goethite which, presumably, displayed greater long-range order than that used in
310 the present study.

311 UV-Vis spectra for untreated batch filtrates are shown in Fig. 5. These spectra reveal
312 two main regions of absorption: a broad, low peak at 400 – 500 nm which is assigned to Fe^{3+}-
313 DFOB, and another peak at 236 nm which is due to the uncomplexed anionic DFOB species,
314 $HDFOB^{2-}$, whose three hydroxamate groups are deprotonated whilst the terminal amine
315 remains protonated (Edwards et al., 2005). We disregard other causes for the peak at 236 nm
316 as UV-Vis scans of reference solutions of SRFA, $Fe(ClO_4)_3$, MOPS/$NaNO_3$, Fe-DFOB, and
317 Fe-SRFA did not show any absorption in this region. Thus, the spectra in Fig. 5 indicate that

318 the untreated filtrates contain both complexed DFOB as Fe^{3+}-DFOB and uncomplexed
319 DFOB.
320 The values of surface excess of DFOB on goethite at 25 °C, pH 6.5 and 270 μM
321 initial siderophore concentration are given in Table 1 (column 4) for the six systems
322 containing both goethite and DFOB. Although we measure surface excess at a single
323 temperature (i.e. 25 °C) Cocozza et al. (2002) report no significant change in surface excess
324 of DFOB on goethite over the temperature range 25 °C to 55 °C for a comparable system.
325 However, the surface excess we calculate for our system 1 (i.e. 14.4 μmol g^{-1}) is nearly five
326 times that observed by Cocozza et al. (2002) (i.e. 2.99 μmol g^{-1}) under comparable
327 conditions. We again attribute this difference to variation in goethite synthesis procedure,
328 with attendant variation in crystallite morphology and density of reactive surface OH groups
329 (Cornell and Schwertmann, 2003).
330 A pseudo-first-order rate coefficient may be used to characterise the kinetics of
331 ligand-promoted dissolution under far from equilibrium conditions as described by Stumm et
332 al. (1987). This approach was applied by Cocozza et al. (2002) to demonstrate the
333 temperature dependence of DFOB mediated goethite dissolution at 55 °C, and the lack of
334 temperature dependence over the range 25 to 40 °C. For the present study, the coefficient (h^{-1})
335 was derived as the ratio of the mass-normalised dissolution rate coefficient to the DFOB
336 surface excess. These values are presented in Table 1 (column 5) and are generally in line
337 with that reported by Kraemer et al. (1999) (i.e. 0.01 h^{-1}). This broad congruence of pseudo-
338 first-order rate coefficients implies that differences in dissolution rate depend principally on
339 DFOB surface excess as influenced by reagent addition sequence.
340
341 ### 3.3. FTIR spectra
342

343 The dominant FTIR vibrations and corresponding assignments for the Fe-free and
344 Fe^{3+}-complexed standards are shown in Table 2. All FTIR absorption peaks produced by our
345 synthetic goethite relate to the structure of goethite. The absence of extraneous peaks
346 indicated that no other phases were present at detectable levels. The FTIR spectrum for our
347 synthetic goethite (Fig. 6) has an absorption band at 640 cm^{-1}, representing the FeO_6 lattice
348 vibrations (Prasad et al., 2006). Other prominent vibrations are the in-plane (δ) and out-of-
349 plane (γ) deformational (bending) modes of hydroxyls at 891 cm^{-1} and 795 cm^{-1}, respectively
350 (cf., Prasad et al. 2006). The broad absorption band located at 3132 cm^{-1} is assigned to the
351 hydroxyl stretch of surface OH, previously reported at 3100 – 3150 cm^{-1} (Cornell and
352 Schwertmann, 2003).
353 In the FTIR spectrum for DFOB the terminal N-H stretching vibrations occur at 3128
354 cm^{-1} and 3325 cm^{-1}, while the vibrational stretching of the amide I band of the C=O group
355 occurs at 1624 cm^{-1} (Cozar et al., 2006; Siebner-Freibach et al., 2006). Another C=O
356 absorption band at 1599 cm^{-1} represents the hydroxamate C=O (cf., Edwards et al., 2005;
357 Domagal-Goldman et al., 2009). An absorption band at 1537 cm^{-1} arises from the
358 superposition of N-H bending and C-N stretching vibrations in the amide II group (cf.,
359 Nightingale and Wagner, 1954) as well as O-H (hydroxamate) in-plane bending vibrations
360 (Cozar et al., 2006). The band at 1480 cm^{-1} is assigned to both the hydroxamate NOH bend
361 and the C-N oxime (hydroxamate resonance structure) stretch corresponding to the 1470 cm^{-1}
362 band of Edwards et al. (2005) (Fig. 6). We also observed a band at 1386 cm^{-1} arising from a
363 combination of vibrational deformation modes in the hydroxamate group and terminal N (cf.,
364 1379 cm^{-1} Edwards et al., 2005). An additional band, at 1047 cm^{-1}, coincides with the
365 hydroxamate N-O resonance of DFOB. However, this band is not due exclusively to DFOB
366 as methanesulfonate, the counter-ion of the DFOB mesylate salt, also shows strong
367 absorption at 1049 cm^{-1} (Borer et al., 2009; Simanova et al., 2010).

368 The FTIR spectrum for SRFA (Fig. 6) displayed two prominent absorption bands, at
369 3425 cm^{-1} and 1720 cm^{-1}, and these were assigned to the phenolic O-H and protonated
370 carboxylic acid C=O vibrational stretching modes, respectively (cf., International Humic
371 Substance Society, 2008). Other absorption bands at 1629 cm^{-1} and 1384 cm^{-1} represent,
372 respectively, the deprotonated asymmetric and symmetric vibrational stretching of
373 carboxylate C=O (cf., Fu and Quan, 2006; Hay and Myneni, 2007). The broad band at 1218
374 cm^{-1}, assigned to the O-H phenolic stretch, was previously observed at 1217 cm^{-1} by Fu and
375 Quan (2006).
376 Complexation between DFOB and Fe^{3+} yields a shift in the amide I band to 1622 cm^{-1}
377 from 1624 cm^{-1} (Fig. 6) as reported by Edwards et al. (2005). The hydroxamate absorption
378 bands at 1537 cm^{-1} and 1480 cm^{-1}, as well as the absorption band at 1386 cm^{-1}, assigned to
379 the hydroxamate near the terminal N, also disappeared upon complexation of DFOB to Fe^{3+}.
380 The Fe^{3+}-DFOB complex gave rise to a new vibrational stretching mode at 1568 cm^{-1},
381 assigned to hydroxamate C=N, and a shift of the existing 1047 cm^{-1} band to 1045 cm^{-1},
382 assigned to hydroxamate N-O (Fig. 6) (Cozar et al., 2006). Upon coordination of
383 hydroxamate oxygen to Fe^{3+}, a new hydroxamate absorption band emerged at 1459 cm^{-1},
384 previously reported at 1455 cm^{-1} by Borer et al. (2009), in a region where bands at 1537 cm^{-1}
385 and 1480 cm^{-1} once appeared (Table 2). The Fe^{3+}-DFOB complex also gives rise to a band at
386 561 cm^{-1}, reported previously at 555 cm^{-1} (Cozar et al., 2006), attributed to the Fe-O
387 stretching vibration, but distinct from the Fe-O stretching of the goethite lattice. Additionally,
388 a broad and intense peak at 3368 cm^{-1}, accompanied by two small shoulders, we attribute to
389 the dissociation of the hydroxamate hydroxyl groups following Fe^{3+} coordination.
390 Following complexation of Fe^{3+} with SRFA, the O-H band at 3425 cm^{-1} becomes
391 broader, and shifts to 3410 cm^{-1} (Fig. 6). In contrast, the COOH and asymmetric C=O bands
392 at 1720 cm^{-1} and 1629 cm^{-1}, respectively, disappeared, whilst new, slightly lower intensity

393 bands appeared at 1687 cm^{-1} and 1631 cm^{-1}. Meanwhile, the peak at 1384 cm^{-1} became
394 sharper and more intense following Fe^{3+} complexation with SRFA (cf., Fu and Quan, 2006),
395 indicating the complexation of carboxylate oxygen to Fe^{3+}.
396 Our FTIR assignments for the DFOB-SRFA and Fe^{3+}-DFOB-SRFA complexes are
397 based on comparison of the FTIR spectra for DFOB, SRFA, Fe^{3+}-DFOB, Fe^{3+}-SRFA, DFOB-
398 SRFA and Fe^{3+}-DFOB-SRFA. Upon formation of the DFOB-SRFA complex, the SRFA
399 phenolic absorption band at 3425 cm^{-1} becomes less intense and slightly broader, shifting to
400 3417 cm^{-1}, while another phenolic band at 1216 cm^{-1} shifted to 1218 cm^{-1} (Fig. 6). The
401 intensity of the prominent SRFA carboxylic C=O band at 1720 cm^{-1} decreased significantly
402 and shifted to 1719 cm^{-1}, whilst the asymmetric C=O band at 1629 cm^{-1} shifted to 1626 cm^{-1}.
403 With respect to the DFOB, bands assigned to the terminal amines shifted from 3128 cm^{-1} and
404 3325 cm^{-1} to a single band at 2939 cm^{-1} of lower intensity.
405 Formation of the Fe^{3+}-DFOB-SRFA complex changed the FTIR spectra for both
406 SRFA and DFOB (Fig. 6). The intensity of the SRFA carboxylic C=O band was reduced,
407 shifting from 1720 to 1723 cm^{-1}, while the SRFA symmetric C=O absorption band at 1384
408 cm^{-1} disappeared. The SRFA phenolic OH band at 1216 cm^{-1} remained largely as it was in
409 the DFOB-SRFA complex, whilst the asymmetric stretching of the carboxylate C=O
410 increased from 1629 cm^{-1} in the Fe-free complex to 1642 cm^{-1} in the Fe^{3+}-DFOB-SRFA
411 complex. The phenolic OH band shifted from 3425 cm^{-1} for the Fe-free SRFA to 3437 cm^{-1}
412 for the Fe^{3+}-DFOB-SRFA complex. The N-O resonance of the hydroxamate group decreased
413 from 1047 cm^{-1} in DFOB to 1042 cm^{-1} in the Fe^{3+}-DFOB-SRFA complex and was
414 accompanied by considerable peak sharpening. Furthermore, the Fe-O vibration at 561 cm^{-1}
415 indicating complexation between Fe^{3+} and DFOB was observed at 542 cm^{-1} in the ternary
416 complex (Fig. 6). Weak bands at 3010 cm^{-1} and 2954 cm^{-1} for the Fe^{3+}-DFOB-SRFA
417 complex are likely due to the decrease in frequency of the N-H group of the terminal N in the

418 DFOB as a result of electrostatic interaction between the DFOB terminal amine and charged
419 SRFA groups.
420
421 # 4. DISCUSSION
422
423 ## 4.1. Sorption of SRFA and DFOB to goethite
424
425 Adsorption of organic matter to iron oxide surfaces occurs by electrostatic
426 interactions, ligand exchange, hydrogen bonding and van der Waals interactions (Sposito,
427 1984). Coulombic attraction of organic solutes to metal oxides can be predicted through
428 construction of a Schindler diagram, a banded rectangle in which the charge properties of the
429 adsorptive and adsorbent are compared as a function of solution pH (Fig. 7) (Schindler,
430 1990). The bottom rectangle displays a horizontal line indicating the pH range over which
431 adsorption is expected to occur based solely on charge. Adsorption occurring outside of this
432 range implies the involvement of specific adsorption mechanisms. On the basis of the
433 Schindler diagram depicted in Fig. 7a, adsorption of SRFA to goethite is predicted over pH ~
434 3 to 9.
435 At pH 6.5 and an initial SRFA concentration of 11.6 mg C L^{-1}, the surface excess of
436 SRFA on goethite was 0.33 mg m^{-2}. This value compares favourably with that reported by
437 Filius et al. (2000) for fulvate adsorption to goethite at pH 7 (i.e. 0.3 mg FA g^{-1}) and also
438 Weng et al. (2006) for their system at pH 5.5 (i.e. 0.4 mg FA g^{-1}). FTIR spectra for the
439 goethite-SRFA surface association were too complex to derive useful molecular-level
440 information concerning adsorption mechanisms. However, FTIR spectra for aqueous Fe^{3+}-
441 SRFA species, when compared with spectra for several reference aqueous complexes (Fig.
442 6), revealed that Fe^{3+} forms inner-sphere complexes with COOH and phenolic OH of SRFA,

443 consistent with that reported in previous studies (Fu and Quan, 2006; Hay and Myeni, 2007).
444 Furthermore, application of the charge distribution multi-site complexation (CD-MUSIC)
445 model provides theoretical evidence that carboxylic groups of SRFA form inner-sphere
446 complexes with Fe via the singly coordinated surface hydroxyls of goethite (i.e. those
447 hydroxyls coordinated to a single Fe^{3+} cation) (Weng et al., 2005; Weng et al., 2006). On the
448 basis of these theoretical predictions and our experimental data, we propose that SRFA binds
449 to the goethite surface via inner-sphere complexation as depicted in Fig. 8, corroborating the
450 work of Filius et al. (2000), who observed inner-sphere adsorption of fulvic acid at pH below
451 the PZC for goethite. Importantly, SRFA adsorption lowers the PZC of goethite and reduces
452 positive surface charge in the vicinity of the adsorption site (Tipping and Cooke, 1982).
453 The Schindler diagram shown in Fig. 7b predicts that goethite can serve as an
454 effective sorbent for DFOB only at pH ~ 8 to 9. However, for our systems at pH 6.5, we
455 observe a surface excess of DFOB ranging from 14.4 to 26.5 μmol g^{-1} (Table 1). Much of this
456 DFOB will be adsorbed via inner-sphere surface complexes (Carrasco et al., 2007), however
457 electrostatic factors may be significant in increasing overall uptake. The predicted
458 electrostatic repulsion at pH 6.5 between DFOB (pK_a ~ 8.6) and the positively charged
459 goethite surface (PZC = 9.2) can be minimised through orientation of the approaching
460 siderophore such that the hydroxamate group furthest from the protonated amine makes first
461 contact with the surface (Cocozza et al., 2002). More significantly, adsorption of the anionic
462 SRFA reduces the positive surface charge of goethite near the site of adsorption (Tipping and
463 Cooke, 1982), thus facilitating localised uptake of DFOB. Consistent with the predicted
464 SRFA enhanced uptake of DFOB, our data show that those systems with both SRFA and
465 DFOB give rise to greater DFOB surface excess than system 1, which contains only DFOB
466 (Table 1).
467

468 4.2. Aqueous complexes

469

470 UV-Vis spectroscopic analysis confirmed the presence of the Fe^{3+}-DFOB complex in
471 supernatant solutions from batch dissolution experiments (Fig. 5). The emergence of FTIR
472 absorption bands at 1459 cm^{-1} and 561 cm^{-1}, assigned to Fe-O (Table 2; Fig. 6), following
473 formation of the Fe^{3+}-DFOB complex provides evidence for presence of the Fe-hydroxamate
474 bond as depicted in Fig. 1b. These observations are consistent with predictions based on the
475 high affinity of desferrioxamine B for the Fe^{3+} cation ($K = 10^{31}$) (Kraemer, 2004).
476 The absence of both soluble Fe and the Fe^{3+}-SRFA species in the supernatant
477 solutions of system 7 indicates that goethite dissolution does not occur at detectable levels in
478 the presence of SRFA alone at pH 6.5 (Fig. 4). However, FTIR analysis of model compounds
479 reveals the diagnostic absorption bands that indicate presence of the Fe^{3+}-SRFA complex, a
480 species that may well form following the liberation of Fe^{3+} by DFOB. The most significant
481 FTIR band arising from the complexation of SRFA with Fe is due to changes in the
482 carboxylate C=O vibration, appearing at 1687 cm^{-1} in Fe^{3+}-SRFA and 1720 cm^{-1} in Fe-free
483 SRFA. Fu and Quan (2006) observed similar changes in C=O vibrations when FA was sorbed
484 to haematite. The other functional group indicative of Fe^{3+}-SRFA bonding, the phenolic OH,
485 changes from 3425 cm^{-1} in the uncomplexed SRFA to 3410 cm^{-1} for Fe^{3+}-SRFA (Table 2).
486 Localisation of Fe within the ternary Fe-DFOB-SRFA complex can help to reveal the
487 mechanisms of goethite dissolution when both organic ligands are present. The FTIR
488 absorption band most diagnostic of Fe complexation by SRFA arises from the carboxylate
489 C=O vibration which, when complexed to Fe, decreases from 1720 cm^{-1} to 1687 cm^{-1}. In the
490 ternary complex this vibration occurs at 1723 cm^{-1} (Table 2), broadly similar to that of the
491 Fe-free SRFA. Furthermore, we observe the main band representing the Fe^{3+}-DFOB
492 complex, the Fe-O vibration, is also present for the Fe-DFOB-SRFA complex, although

493 occurring at the somewhat lower frequency of 542 cm^{-1}. On the basis of these spectroscopic
494 observations we infer that Fe in the ternary complex is bound only to the hydroxamate groups
495 of DFOB. Thus, in the presence of both DFOB and SRFA, dissolved Fe^{3+} is complexed by
496 DFOB rather than SRFA, consistent with our observations, and as predicted by the much
497 higher affinity of Fe^{3+} for DFOB than for SRFA at pH 6.5 (Pandeya, 1993; Kraemer, 2004;
498 Muller and Batchelli, 2011). The FTIR spectrum for Fe-DFOB-SRFA also shows notable
499 increases in wavenumber for SRFA phenolic OH (3437 cm^{-1}) and C=O (1642 cm^{-1}),
500 compared to their uncomplexed form (Table 2). However, we believe these wavenumber
501 shifts are not due to Fe complexation by SRFA but rather to ring strain caused by a change in
502 SRFA conformation to accommodate the DFOB molecule as the Fe-O complex forms
503 (Sharma, 2007).
504 FTIR data show that SRFA and DFOB combine to form intimate associations in
505 aqueous solution. Specifically, bonding between the SRFA phenolic OH and the residual
506 positive charge on the DFOB terminal NH_3 group yields a significant wavenumber change
507 for these groups, shifting the uncomplexed SRFA phenolic OH from 3425 cm^{-1} to 3417 cm^{-1}
508 in the DFOB-SRFA complex (Table 2). Curiously, the SRFA phenolic OH appears to
509 dominate these associations, despite the greater population of carboxyl groups within this
510 humic material, with reports of carboxyl:phenol molar ratios varying from 3:2 (Alvarez-
511 Puebla et al., 2006) to 4:1 (Ritchie and Perdue, 2003). The FTIR bands for the DFOB
512 terminal NH_3 group vibrations display even greater wavenumber shifts, from 3128 cm^{-1} and
513 3325 cm^{-1} in the uncomplexed siderophore to a single absorption peak at 2939 cm^{-1} in the
514 DFOB-SRFA complex.
515
516 4.3. Influence of DFOB and SRFA on goethite dissolution
517

518 DFOB adsorbs to goethite principally via inner-sphere surface complexes (Carrasco et
519 al., 2007), the necessary first step in ligand-controlled dissolution. The rate law for ligand-
520 controlled dissolution predicts that the mass-normalised dissolution rate of goethite, R_{DFOB},
521 will be proportional to the DFOB surface excess, n_{DFOB}:
522
523 $$R_{DFOB} = k_{DFOB}\, n_{DFOB}$$
524
525 where k_{DFOB} is a pseudo first-order rate coefficient. The dissolution of goethite by
526 siderophores obeys this rate law under many experimental conditions, even in the presence of
527 low MW organic ligands such as oxalate (Cheah et al., 2003). Our values for k_{DFOB} show
528 little variation irrespective of treatment (0.012 – 0.020 h^{-1}) (Table 1, column 5) and are
529 broadly in line with that reported by Kraemer et al. (1999) (i.e. 0.01 h^{-1}). However, the
530 pseudo first-order rate coefficient for dissolution of goethite by DFO-D1, the acetyl
531 derivative of DFOB, increases to 0.05 h^{-1} (Kraemer et al., 1999) while that for a simple
532 monohydroxamate ligand, acetohydroxamic acid, was calculated as 0.073 h^{-1} (Holmén and
533 Casey, 1998).
534 In the present study, Fe release from goethite increased with the addition of SRFA,
535 particularly where SRFA is added prior to DFOB (systems 4 and 5), and further still when
536 SRFA is introduced as the DFOB-SRFA complex (system 6) (Fig. 4). A quantitative
537 assessment of the effect of SRFA presence on goethite dissolution can obtained through
538 comparison of the mass-normalised zero-order rate coefficients (Table 1, column 3). The rate
539 coefficients for systems 4 (0.364 μmol g^{-1} h^{-1}) and 5 (0.412 μmol g^{-1} h^{-1}) are 40 to 60% larger
540 than that for system 1 (0.257 μmol g^{-1} h^{-1}), while the coefficient for system 6 (0.440 μmol g^{-1}
541 h^{-1}) is nearly 70% larger than for the SRFA-free system.

542 Despite the positive influence of SRFA on goethite dissolution by means of increased
543 adsorption of DFOB (compare DFOB surface excess for system 1 with that for systems 2 – 6;
544 Table 1, column 4), the rate of Fe release does not correlate linearly with DFOB surface
545 excess. This nonlinear relationship between DFOB adsorption and goethite dissolution may
546 reflect changes in surface speciation of DFOB when SRFA is present. The SRFA induced
547 reduction in positive surface charge enables greater electrostatic adsorption of DFOB as
548 predicted by Tipping and Cooke (1982). However, as formation of a DFOB inner-sphere
549 complex is the required first step in ligand-controlled dissolution of goethite, DFOB held
550 non-specifically through Coulombic forces would not contribute to goethite dissolution.
551 Furthermore, in the case of system 6, inner-sphere complexation of DFOB to goethite may be
552 partly limited by the rate at which DFOB and SRFA decouple. Nevertheless, the effect of
553 SRFA presence on the DFOB-goethite system has important implications for the microbial
554 acquisition of Fe in soils and other humic rich environments. Data in Fig. 4 show that for
555 nearly all systems the efficacy of DFOB is increased with SRFA presence. For example, at
556 reaction times of 120 and 330 h, system 1 (with only DFOB) yields 34.7 and 70.3 μM Fe
557 while system 6 (containing both DFOB and SRFA) yields 71.6 and 125.7 μM Fe,
558 respectively (Fig. 4). Thus, the benefit to the microbe producing the siderophore is
559 substantial, and this advantage is achieved with little or no energetic cost to the organism.
560
561 ### 4.4. Mechanism of SRFA enhanced goethite dissolution
562
563 Various mechanisms have been proposed to explain the effect of low MW organic
564 acids on goethite dissolution by DFOB. For example, in their examination of the oxalate-
565 DFOB-goethite system at pH 5, Cheah et al. (2003) suggest that Fe solubilised from the
566 goethite surface by oxalate is subsequently wrested from the Fe^{3+}-oxalate aqueous complex

567 by DFOB. Given sufficient DFOB to complex soluble Fe, oxalate will thus be liberated to
568 react once again with the goethite surface. Reichard et al. (2007a), also examining the
569 oxalate-DFOB-goethite system, proposed a dissolution mechanism broadly similar to that of
570 Cheah et al. (2003), except that the former workers identified two distinct pools of labile Fe,
571 namely, (i) Fe^{3+} present as a residuum of goethite synthesis and (ii) kinetically labile Fe^{3+}
572 coordinated to unshared hydroxyls. The mechanism we propose here for the dissolution of
573 goethite in the presence of DFOB and the higher MW organic compound, SRFA, differs from
574 those proposed for oxalate in that SRFA plays a largely indirect, though no less important
575 role in increasing the efficacy of DFOB. Adsorbed SRFA reduces the net positive surface
576 charge of goethite, thereby increasing DFOB uptake, and also, through formation of Fe
577 complexes with fulvic carboxyl and phenol groups, increases the pool of labile surface Fe.
578 Our model for goethite dissolution by DFOB in the presence of SRFA, illustrated in Fig. 9, is
579 summarised below:
580
581 (i) surface Fe of goethite is coordinated to SRFA via carboxylic (GOE)Fe^{3+}-$^{-}$OOC(SRFA) or
582 phenolic (GOE)Fe^{3+}-$^{-}$O(SRFA) functional groups through ligand exchange;
583
584 (ii) the Fe^{3+}-SRFA attachment destabilises Fe-O bonds at the goethite surface, leading to
585 labilisation of Fe^{3+};
586
587 (iii) adsorbed SRFA locally reduces the positive charge on the goethite surface, thereby
588 enhancing $DFOB^{+}$ uptake;
589
590 (iv) protons are displaced from the hydroxamate groups of DFOB as these groups bind to the
591 labile Fe^{3+} via ligand exchange;

592

593 (vi) the Fe^{3+}-$DFOB^{+}$ complex is released to solution where it remains a free species or
594 subsequently complexes with aqueous SRFA.

595

596 ## 5. CONCLUSIONS

597

598 Our results show that dissolution of goethite by DFOB is enhanced considerably
599 through the presence of FA, particularly when FA sorption preceeds that of DFOB, or when
600 the two organic compounds are sorbed simultaneously. Importantly, our batch dissolution
601 experiments incorporating FA reveal a more complex picture of siderophore function than is
602 portrayed in the current literature. This humic material is revealed as a catalyst for goethite
603 dissolution, in the sense that FA enhances the efficacy of DFOB but is itself not directly
604 involved in Fe solubilisation. This work shines important new light on the factors influencing
605 Fe acquisition by microorganisms and plants in soils and sediments, environments in which
606 humic materials are ubiquitous. The incorporation of natural organic matter such as FA into
607 geochemical models of siderophore function is therefore essential to more accurately predict
608 the geochemical cycling of Fe in these natural environments.

609

610

611 ## ACKNOWLEDGEMENTS

612

613 Funding for this study was provided through a Birkbeck, University of London, Research
614 Studentship and from The Natural History Museum. We thank the following for their
615 generous assistance: Stanislav Strekopytov, Catherine Unsworth and Emma Williams for
616 chemical analysis, Agnieszka Dybowska and Hazel Hunter for FTIR spectroscopy, Alex Ball

617 for SEM analysis and photography, Superb Misra for AFM analysis and photography, and
618 Jens Najorka for XRD analysis.
619

620 ## REFERENCES

621

622 Alvarez-Puebla R.A., Valenzuela-Calahorro C. and Garrido J.J. (2006) Theoretical study on
623 fulvic acid structure, conformation and aggregation - A molecular modelling approach.
624 *Sci. Total Environ.* 358, 243–254.
625 Borer P., Hug S.J., Sulzberger B., Kraemer S.M. and Kretzschmar R. (2009) ATR-FTIR
626 spectroscopic study of the adsorption of desferrioxamine B and aerobactin to the surface
627 of lepidocrocite (γ-FeOOH). *Geochim.Cosmochim. Acta* 73, 4661-4672.
628 Brantley S.L. and Chen Y. (1995) Chemical weathering rates of pyroxenes and amphiboles.
629 *Rev. Mineral.* 31, 119-172.
630 Carrasco N., Kretzschmar R., Pesch M.-L. and Kraemer S.M. (2007) Low concentrations of
631 surfactants enhance siderophore-promoted dissolution of goethite. *Environ. Sci. Technol.*
632 41, 3633-3638.
633 Cervini-Silva J. (2008) Adsorption of trihydroxamate and catecholate siderophores on alpha-
634 iron (hydr)oxides and their dissolution at pH 3.0 to 6.0. *Soil Sci. Soc. Am. J.* 72, 1557-
635 1562.
636 Cheah S., Kraemer S.M., Cervini-Silva J. and Sposito G. (2003) Steady-state dissolution
637 kinetics of goethite in the presence of desferrioxamine B and oxalate ligands: implications
638 for the microbial acquisition of iron. *Chem. Geol.* 198, 63-75.
639 Chin Y., Aiken G. and O'Loughlin E. (1994) Molecular weight, polydispersity, and
640 spectroscopic properties of aquatic humic substances. *Environ. Sci. Technol.* 28, 1853–
641 1858.

642 Cocozza C., Tsao C.C.G., Cheah F., Kraemer S.M., Raymond K.N., Miano T.M. and Sposito
643 G. (2002) Temperature dependence of goethite dissolution promoted by trihydroxamate
644 siderophores. *Geochim.Cosmochim. Acta* 66, 431-438.
645 Colnaghi Simionato A.V., Cantú M.D. and Carrilho E. (2006) Characterization of metal-
646 deferroxamine complexes by continuous variation method: A new approach using
647 capillary zone electrophoresis. *Microchem. J.* 82, 214-219.
648 Cornell R.M., Posner A.M. and Quirk J.P. (1974) Crystal morphology and the dissolution of
649 goethite. *J. Inorg. Nucl. Chem.* 36, 1937-1946.
650 Cornell R.M. and Schwertmann U. (2003) *The Iron Oxides - Structure, Properties, Reactions,*
651 *Occurences and Uses*, Second Edition. Wiley-VCH, New York.
652 Cozar O., Leopold N., Jelic C., Chis V., David L., Mocanu A. and Tomoaia-Cotisel M.
653 (2006) IR, Raman and surface-enhanced Raman study of desferrioxamine B and its Fe(III)
654 complex, ferrioxamine B. *J. Mol. Struct.* 788, 1-6.
655 Cramer S.M., Bryon N. and Csaba H. (1984) High-performance liquid chromatography of
656 deferroxamine and ferrioxamine: interference by iron present in the chromatographic
657 system. *J. Chromatogr. A* 295, 405–411.
658 Dhungana S., White P.S. and Crumblis A.L. (2001) Crystal structure of ferrioxamine B: a
659 comparative analysis and implications for molecular recognition. *J. Biol. Inorg. Chem.* 8,
660 810–818.
661 Domagal-Goldman S.D., Paul K.W., Sparks D.L. and Kubicki J.D. (2009) Quantum chemical
662 study of the Fe(III)-desferrioxamine B siderophore complex - Electronic structure,
663 vibrational frequencies, and equilibrium Fe-isotope fractionation. *Geochim. Cosmochim.*
664 *Acta* 73, 1-12.
665 Dubbin W.E. and Ander E.L. (2003) Influence of microbial hydroxamate siderophores on
666 Pb(II) desorption from α-FeOOH. *Applied Geochemistry* 18, 1751-1756.

667 Edwards D.C., Nielsen S.B., Jarzecki A.A., Spiro T.G. and Myneni S.C.B. (2005)
668 Experimental and theoretical vibrational spectroscopy studies of acetohydroxamic acid
669 and desferrioxamine B in aqueous solution: Effects of pH and iron complexation.
670 *Geochim.Cosmochim. Acta* 69, 3237-3248.
671 Filius J.D., Lumsdon D.G., Meeussen J.C.L., Hiemstra T. and van Riemsdijk W.H. (2000)
672 Adsorption of fulvic acid on goethite. *Geochim.Cosmochim. Acta* 64, 51-60.
673 Filius J.D., Meeussen J.C.L., Lumsdon D.G., Hiemstra T. and van Riemsdijk W.H. (2003)
674 Modeling the binding of fulvic acid by goethite: the speciation of adsorbed FA molecules.
675 *Geochim.Cosmochim. Acta* 67, 1463-1474.
676 Fu H. and Quan X. (2006) Complexes of fulvic acid on the surface of hematite, goethite, and
677 akaganeite: FTIR observation. *Chemosphere* 63, 403-410.
678 Gan D., Kotob S.I. and Walia D.S. (2007) Evaluation of a spectrophotometric method for
679 practical and cost effective quantification of fulvic acid. *Ann. Environ. Sci.* 1, 11–15.
680 Ghabbour E.A. and Davies G. (2009) Spectrophotometric analysis of fulvic acid solutions - A
681 second look. *Ann. Environ. Sci.* 3, 131–138.
682 Haselwandter K. (2008) Structure and function of siderophores produced by mycorrhizal
683 fungi. *Mineral. Mag.* 72, 61-64.
684 Hay M.B. and Myneni S.C.B. (2007) Structural environments of carboxylic groups in natural
685 organic molecules from terrestial systems. Part 1: infrared spectroscopy.
686 *Geochim.Cosmochim. Acta* 71, 3518-3532.
687 Holmén B.A. and Casey W.H. (1996) Hydroxamate ligands, surface chemistry and the
688 mechanism of ligand promoted dissolution of goethite [α-FeOOH(s)].
689 *Geochim.Cosmochim. Acta* 60, 4403-4416.

690 Holmén B.A. and Casey W.H. (1998) Erratum to Hydroxamate ligands, surface chemistry
691 and the mechanism of ligand promoted dissolution of goethite [α-FeOOH(s)].
692 *Geochim.Cosmochim. Acta* 62, 726.
693 International Humic Substance Society (2008) FTIR spectra were measured at the Instituto di
694 Chimica Agraria, Università di Bari, Bari, Italy. [online] Available at:
695 <http://www.humicsubstances.org/spectra.html> [Accessed on 25th June, 2012].
696 Kosmulski M., Durand-Vidal S., Maczaka E. and Rosenholm J. (2004) Morphology of
697 synthetic goethite particles. *J. Colloid Interf. Sci*. 271, 261-269.
698 Kraemer S.M. (2004) Iron oxide dissolution and solubility in the presence of siderophores.
699 *Aquat. Sci*. 66, 3-18.
700 Kraemer S.M., Cheah S., Zapf R., Xu J., Raymond K.N. and Sposito G. (1999) Effect of
701 hydroxamate siderophore on Fe release and Pb(II) adsorption by goethite.
702 *Geochim.Cosmochim. Acta* 63, 3003-3008.
703 Lasaga A.C. (1998) *Kinetic Theory in the Earth Sciences*. Princeton University Press.
704 Liermann L.J., Kalinowski B.E., Brantley S.L. and Ferry J.G. (2000) Role of bacterial
705 siderophores in dissolution of hornblende. *Geochim.Cosmochim. Acta* 64, 587-602.
706 Muller F. and Batchelli S. (2011) Binding of iron and copper to humic colloids in the Thurso
707 River plume. *Geophys. Res. Abstr*. 13, EGU2011-8132.
708 Nightingale R.E., Wagner E.L. (1954) The vibrational spectra and structure of solid
709 hydroxylamine and deutero-hydroxylamine. *J. Chem. Phys*. 22, 203–207.
710 Pandeya S.B. (1993) Ligand competition method for determining stability constants of fulvic
711 acid iron complexes. *Geoderma* 58, 219–231.
712 Powell P.E., Cline G.R., Reid C.P.P. and Szanislo P.J. (1980) Occurrence of hydroxamate
713 siderophore iron chelators in soils. *Nature* 287, 833–834.

714 Prasad P.S.R., Prasad K.S., Chaitanya V.K., Babu E.V.S.S.K., Sreedhar B. and Murthy S.R.
715 (2006) In situ FTIR study on the dehydration of natural goethite. *J. Asian Earth Sci.* 27,
716 503-511.
717 Qu J.-H., Liu H.-J., Liu S.-X. and Lei P.J. (2003) Reduction of fulvic acid in drinking water
718 by ferrate. *J Environ. Eng.-ASCE* 129, 17-24.
719 Raymond K.N. and Dertz E.A. (2004) Biochemical and physical properties of siderophores.
720 In *Iron Transport in Bacteria* (eds. A.R. Mew, S.M. Payne and J.H. Crosa). ASM Press,
721 Washington, pp. 3 - 17.
722 Reichard P.U., Kretzschmar R. and Kraemer S.M. (2007a) Dissolution mechanisms of
723 goethite in the presence of siderophores and organic acids. *Geochim.Cosmochim. Acta* 71,
724 5635-5650.
725 Reichard P.U., Kretzschmar R. and Kraemer S.M. (2007b) Rate laws of steady-state and non-
726 steady-state ligand-controlled dissolution of goethite. *Colloid Surface A* 306, 22-28.
727 Ritchie J.D. and Perdue E.M. (2003) Proton-binding study of standard and reference fulvic
728 acid, humic acids, and natural organic matter. *Geochim.Cosmochim. Acta* 67, 85-96.
729 Schindler P.W. (1990) Co-adsorption of Metal Ions and Organic Ligands: Formation of
730 Ternary Complexes. In *Mineralogy Volume 23 Mineral-Water Interface Geochemistry*
731 (eds. M.F. Hochella and A.F. White). Mineralogical Society of America,Washington, DC.
732 Chapter 7.
733 Schwertmann U. and Cornell R.M. (1991) *Iron Oxides in the Laboratory: Preparation and*
734 *Characterisation*. VCH Publishers, New York.
735 Sharma B.K. (2007) *Fundamental Principles of Spectroscopy*. Krishna Prakashan Media Ltd,
736 Delhi.

737 Siebner-Freibach H., Hadar Y., Yariv S., Lapides I. and Chen Y. (2006)
738 Thermospectroscopic study of the adsorption mechanism of the hydroxamic siderophore
739 ferrioxamine B by calcium montmorillonite. *J Agric Food Chem.* 54, 1399-1408.
740 Simanova A.A., Persson P. and Loring J.S. (2010) Evidence for hydrolysis and Fe(III)
741 reduction in the dissolution of goethite by desferrioxamine-B. *Geochim.Cosmochim. Acta*
742 74, 6706-6720.
743 Sposito G. (1984) *The Surface Chemistry of Soils*. Oxford University Press, New York.
744 Sposito G. (1994) *Chemical Equilibria and Kinetics in Soils*. Oxford University Press, New
745 York. .
746 Stevenson R.J. (1985) Geochemistry of Soil Humic Substances. In *Humic Substances in Soil,*
747 *Sediment and Water- Geochemistry, Isolation and Characterisation* (eds. G.R. Aiken,
748 D.M. McKnight and R.L. Wershaw). John Wiley and Sons, New York.
749 Stumm W., Wehrli B. and Wieland E. (1987) Surface complexation and its impact on
750 geochemical kinetics. *Croat. Chem. Acta* 50, 1861-1869.
751 Tatár E., Mihucz V.G., Zámbó L., Gasparics T. and Záray G. (2004) Seasonal changes of
752 fulvic acid, Ca and Mg concentrations of water samples collected above and in the Béke
753 Cave of the Aggtelek karst system (Hungary). *Appl. Geochem.* 19, 1727-1733.
754 Tipping E. and Cooke D. (1982) The effects of adsorbed humic substances on the surface
755 charge of goethite (α-FeOOH) in fresh waters. *Geochim.Cosmochim. Acta* 46, 75-80.
756 Watteau F. and Berthelin J. (1994) Microbial dissolution of iron and aluminium from soil
757 minerals: efficiency and specificity of hydroxamate siderophores compared to aliphatic
758 acids. *Eur. J. Soil Biol.* 30, 1–9.
759 Weng L.P., Koopal L.K., Hiemstra T., Meeussen J.C.L. and Van Riemsdijk W.H. (2005)
760 Interactions of calcium and fulvic acid at the goethite-water interface.
761 *Geochim.Cosmochim. Acta* 69, 325-339.

762 Weng L.P., Van Riemsdijk W.H., Koopal L.K. and Hiemstra T. (2006) Adsorption of humic
763 substances on goethite: Comparison between humic acids and fulvic acids. *Environ. Sci.*
764 *Technol.* 40, 7494-7500.
765 Whitnall M. and Richardson D.R. (2006) Iron: A new target for pharmacological intervention
766 in neurodegenerative diseases. *Semin. Pediatr. Neurol.* 13, 186–187.
767
768
769
770
771
772
773
774
775
776
777
778
779
780
781
782
783
784
785
786

Figure Captions

Figure 1. (a) Structural representation of desferrioxamine-B (DFOB). The terminating R group (i) is an amine (pK_a = 10.9). The three hydroxyl groups (ii – iv) have pK_a values of 9.8, 9.2 and 8.6, respectively (Colnaghi Simionato et al., 2006). The hydroxamate (oxime) group is shown along with the amide I (C=O) and amide II (N-H and C-N). Adapted from Whitnall and Richardson (2006). (b) Structure of DFOB bound to Fe^{3+} as ferrioxamine B. DFOB is hexadentate, giving a complex with Fe^{3+} comprised of three, five-membered rings. Adapted from Cramer et al. (1984).

Figure 2. Generalised depiction of the proposed molecular structure of FA based on the Temple-Northeastern-Birmingham (TNB) molecular modelling programme (Alvarez-Puebla et al. (2006), in accordance with the experimentally derived elemental composition, number and type of acidic groups, and molecular weight of FA.

Figure 3. Graphical representation showing the permutations of the batch dissolution of goethite with DFOB and SRFA as a function of reaction duration.

Figure 4. Iron release by goethite in the presence of only DFOB (system 1) and both DFOB and SRFA (systems 2 – 6), with permutations as described in Fig. 3. System 7 is a goethite-SRFA suspension; system 8 is a goethite suspension lacking any organic ligand. Systems 9 and 10 are solutions of DFOB and SRFA, respectively, and serve as controls. Initial siderophore concentration: 270 μM; solid concentration: 0.7 g L^{-1}; pH 6.5.

812

813 Figure 5. UV-Vis spectra of untreated filtrate solutions showing absorbance for uncomplexed
814 DFOB (270 μM) near 236 nm and absorbance for the Fe-DFOB complex appearing as a low,
815 broad peak at 400 – 500 nm.

816

817 Figure 6. FTIR spectra for synthetic goethite, DFOB, SRFA, Fe-DFOB, Fe-SRFA, DFOB-
818 SRFA and Fe-DFOB-SRFA. Reference compounds have the following molar ratios:-
819 Fe:DFOB (2:1), Fe:SRFA (5:1), DFOB:SRFA (1:1) and Fe:DFOB:SRFA (5:1:1). See Table
820 2 for peak assignments.

821

822 Figure 7. Schindler diagrams illustrating the charge properties of goethite and ionic SRFA
823 and DFOB. The horizontal bar in the bottom rectangle indicates the pH range over which
824 purely electrostatic adsorption mechanisms are possible.

825

826 Figure 8. Proposed adsorption mechanism for the goethite-SRFA complex, involving a
827 chelate ring incorporating COO^- and phenolic OH from SRFA.

828

829 Figure 9. Proposed mechanism of goethite dissolution in the presence of DFOB and SRFA.

830

831

Table 1

Table 1. Linear regression equations, mass-normalised zero-order dissolution rate coefficients, surface excess values for DFOB, and pseudo-first-order rate coefficients for goethite dissolution at pH 6.5 and 25°C.

System	Regression equation	Rate coefficient (μmol g^{-1} h^{-1})	DFOB surface excess (μmol g^{-1})	Pseudo-first-order rate coefficient (h^{-1})
1	Y = 0.180X + 11.90	0.257 $\pm$ 0.016	14.4	0.018
2	Y = 0.191X + 14.94	0.273 $\pm$ 0.009	19.0	0.014
3	Y = 0.188X + 10.00	0.268 $\pm$ 0.034	23.3	0.012
4	Y = 0.255X + 14.66	0.364 $\pm$ 0.014	18.3	0.020
5	Y = 0.289X + 14.08	0.412 $\pm$ 0.000	26.5	0.016
6	Y = 0.308X + 29.72	0.440 $\pm$ 0.070	22.8	0.019

Initial DFOB concentration = 270 μM
Goethite concentration = 0.7 g L^{-1}
Y = soluble Fe (μM)
X = time (h)

Table 2

Table 2. FTIR absorption bands (cm^{-1}) and their assignments for DFOB, synthetic goethite, SRFA and four complexes: Fe-DFOB, Fe-SRFA, DFOB-SRFA and Fe-DFOB-SRFA. Assignments are based on Cornell and Schwertmann (2003); Edwards et al. (2005); Cozar et al. (2006); Prasad et al. (2006); and Borer et al. (2009). Vibration modes are designated as follows: ν, stretching; δ, deformation; s, symmetrical; as, asymmetric.

Assignment	DFOB	Goethite	SRFA	Fe-DFOB	Fe-SRFA	DFOB-SRFA	Fe-DFOB-SRFA
$\nu_{C=O}$ amide I	1624			1622		1624	
$\nu_{C=O}$ hydroxamate	1599						
$\nu_{C=N}$ hydroxamate (resonance)				1568			
δ_{N-H}, ν_{C-N} amide II	1537						
δ_{NOH}, ν_{C-N}, ν_{C-N} hydroxamate X2, adjacent to hydroxamate	1480						
ν_{Fe-O} hydroxamate-iron				1459			
ν_{C-N}, δ_{C-H}, δ_{N-H} hydroxamate X2, terminal N	1386						
ν_{N-O} hydroxamate (resonance)	1047			1045		1046	1042
ν_{Fe-O} hydroxamate-iron				561			542
ν_{OH} (phenolic)			3425		3410	3417	3437
ν_{N-H} (terminal N)	3128 3325			3368		2939	3010 2954
$\nu_{C=O}$ carboxylic acid protonated			1720		1687	1719	1723
$\nu_{as\ C=O}$ carboxylic acid deprotonated			1629		1631	1626	1642
$\nu_{s\ C=O}$ carboxylic acid deprotonated			1384		1384	1385	
ν_{OH} phenolic			1218			1218	1216
$\nu_{(OH)}$ hydroxyl stretch		3132					
δ_{OH} in-plane-hydroxyl		891					
δ_{OH} out-of-plane hydroxyl		795					
ν_{FeO6} lattice mode		640					

Figure 1

Click here to download high resolution image

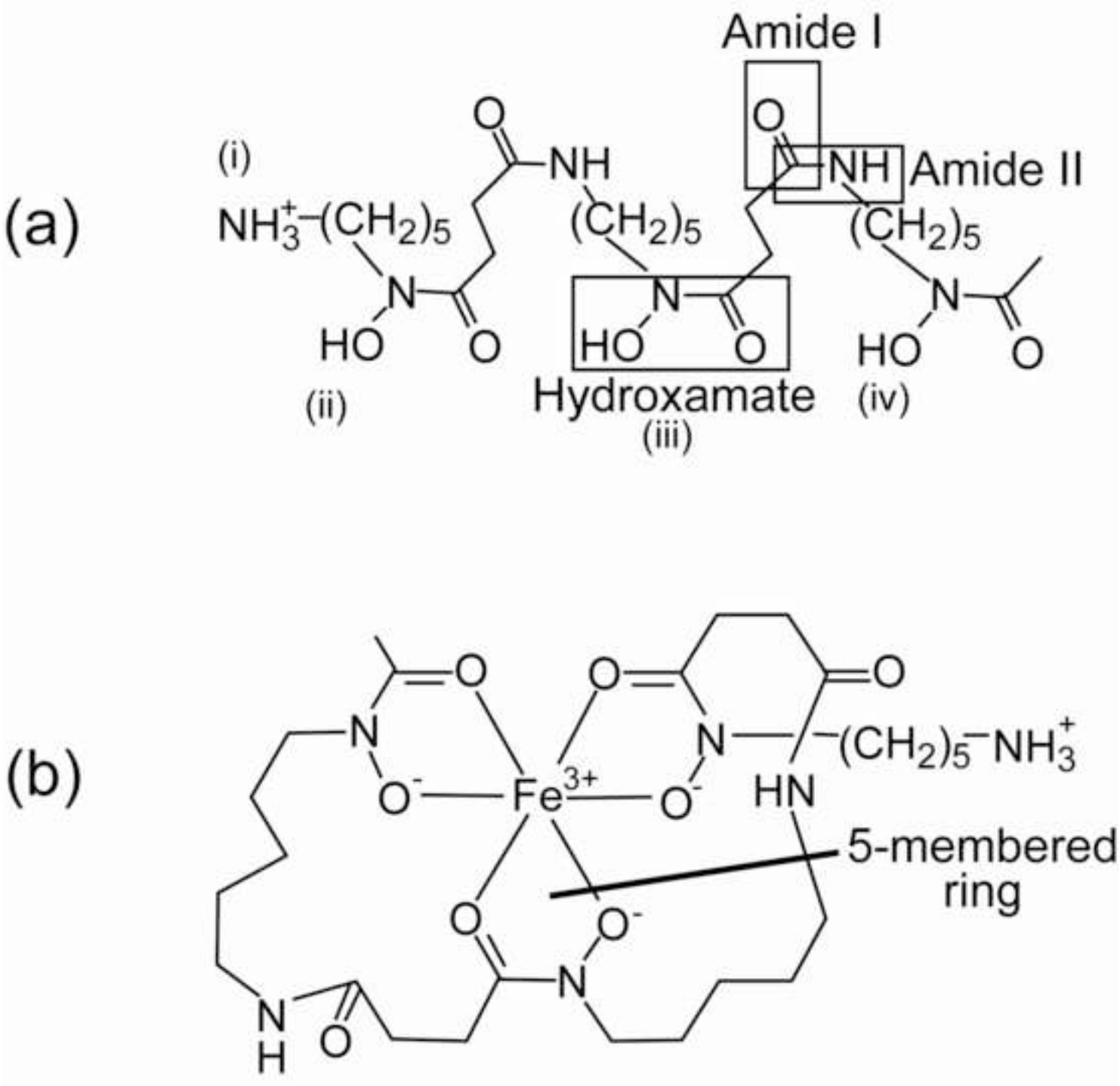

Figure 2

Click here to download high resolution image

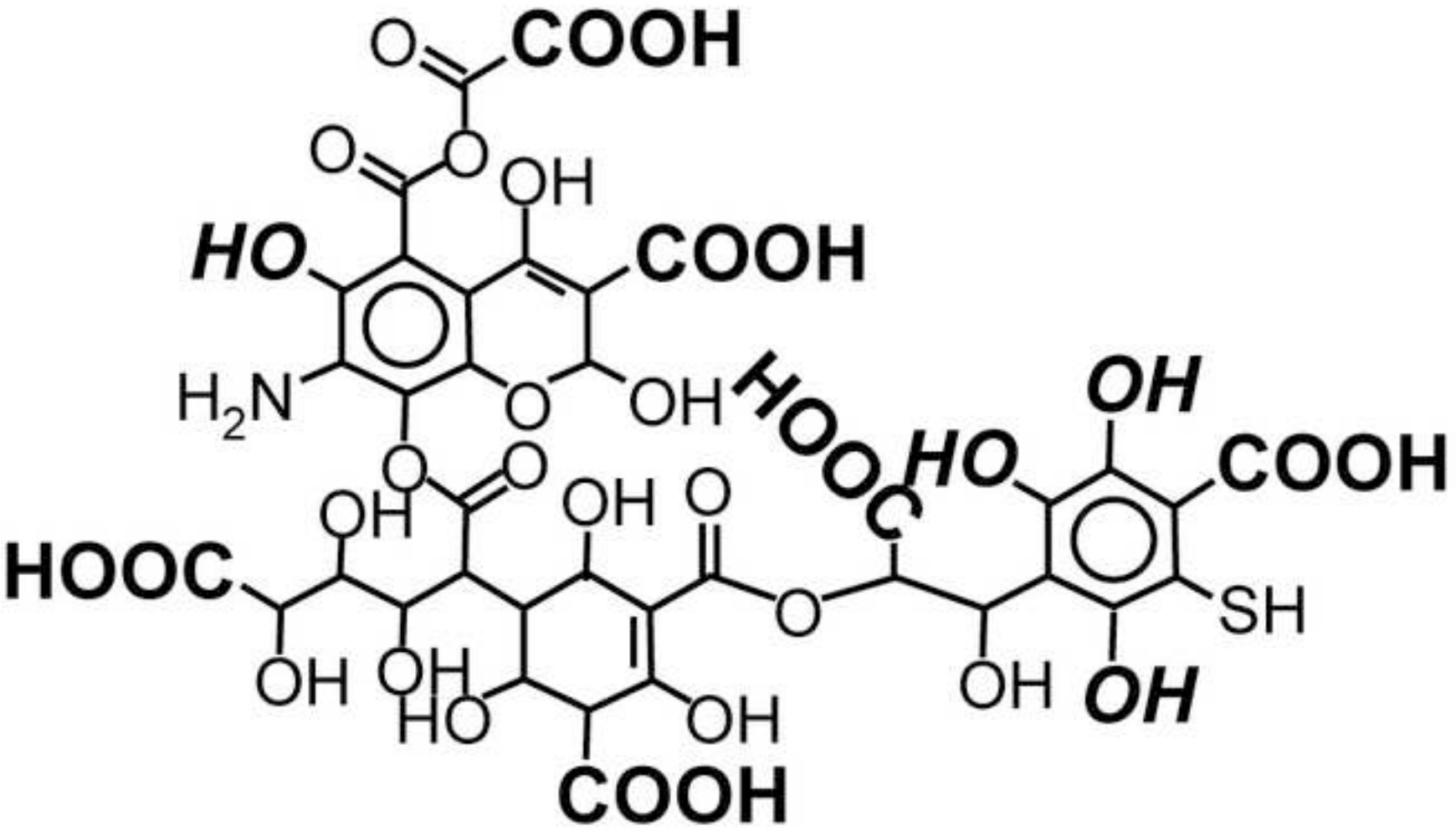

Phenolic group: $(C_6H_5)OH$, $HO(H_5C_6)$

Carboxylic acid group: **COOH, HOOC**

Figure 3

Click here to download high resolution image

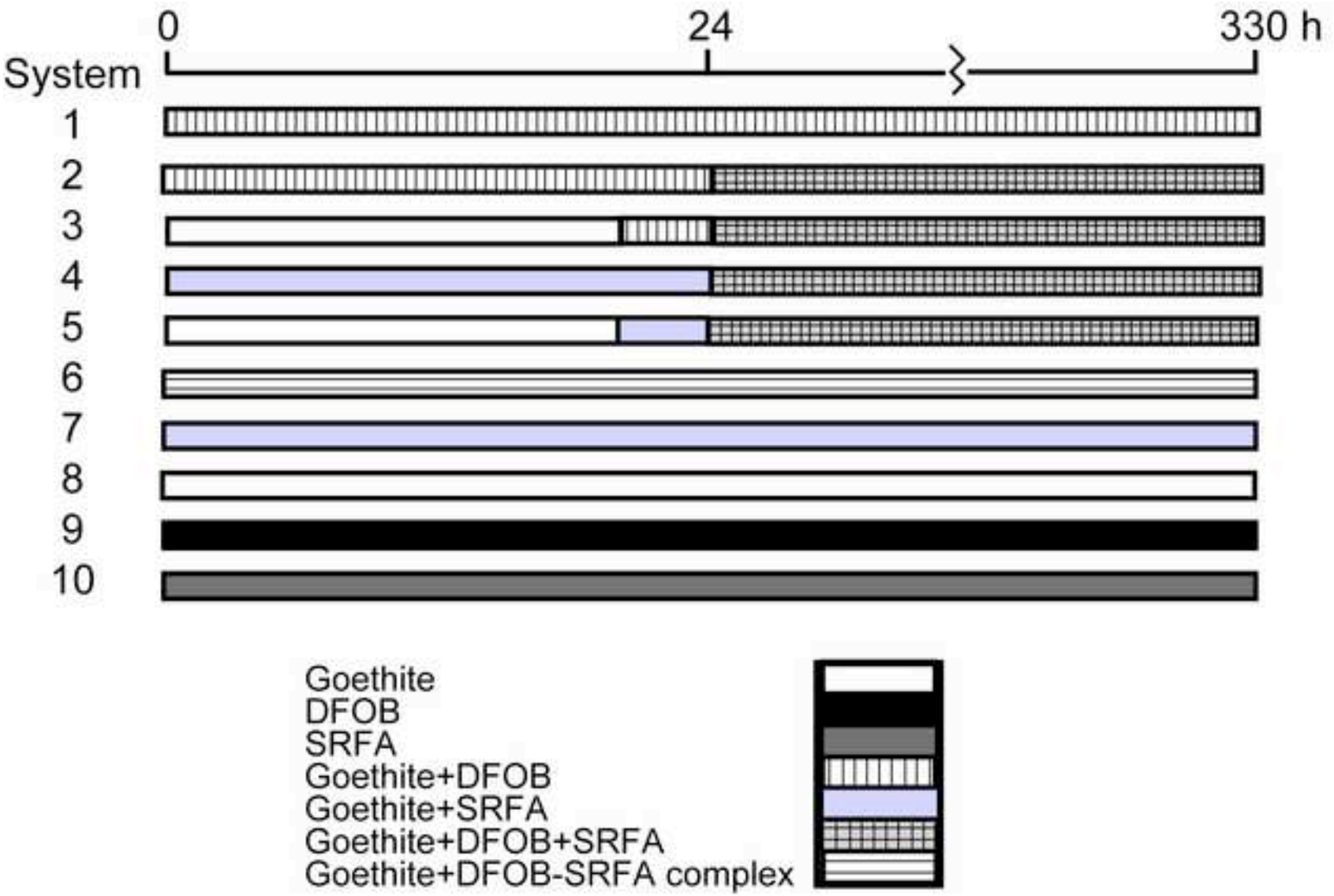

Figure 4

Click here to download high resolution image

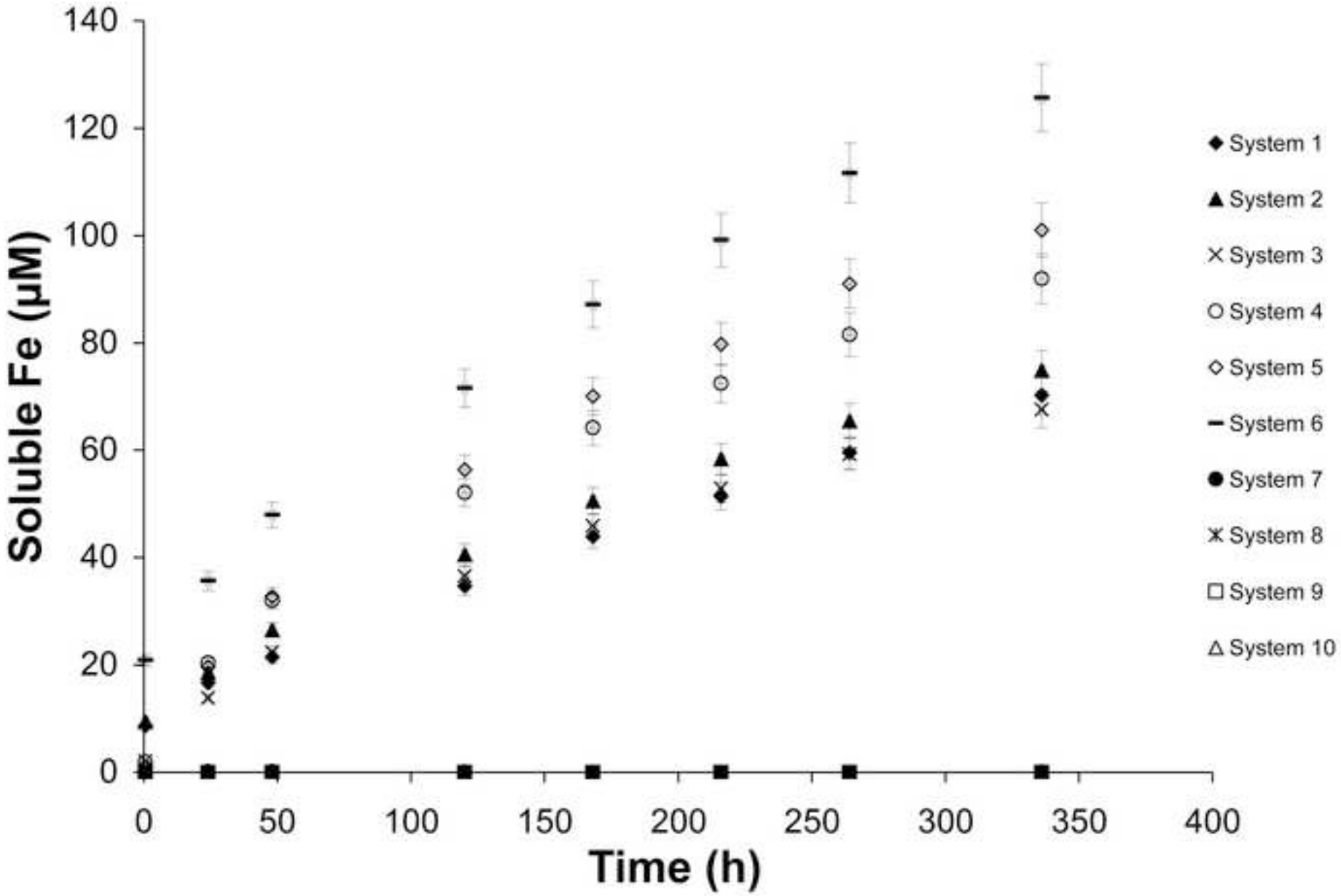

Figure 5

Click here to download high resolution image

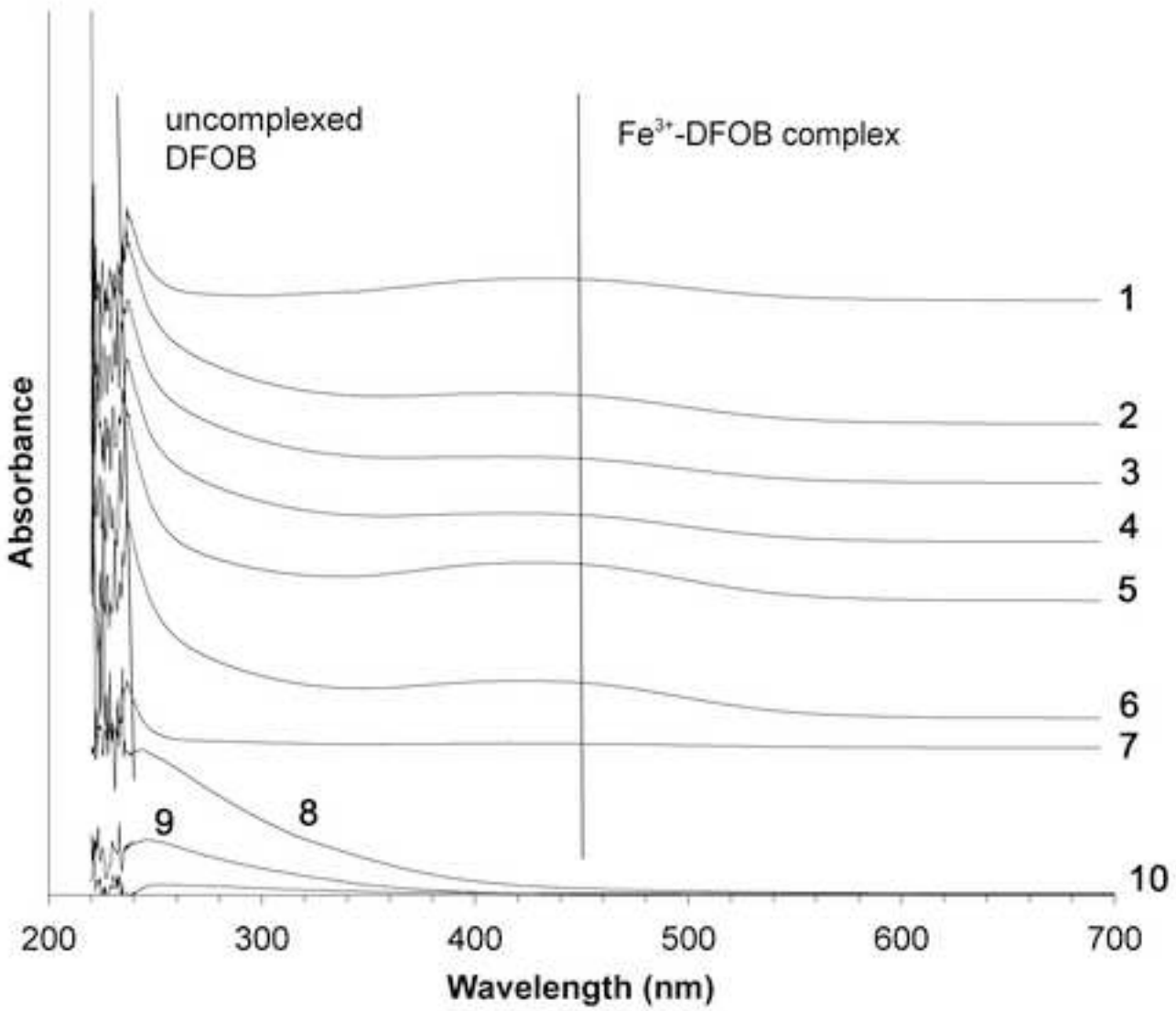

Figure 6

Click here to download high resolution image

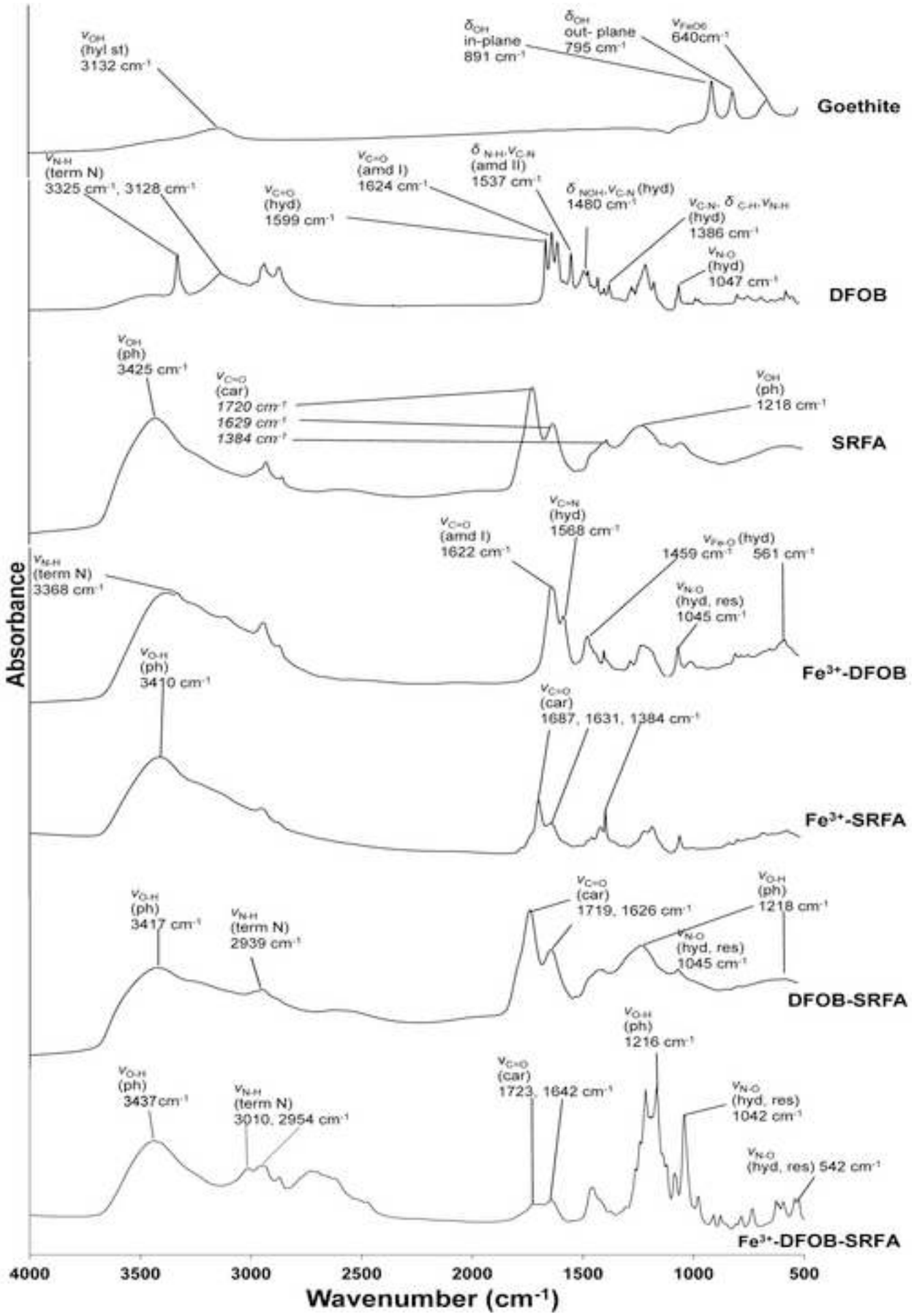

Figure 7

Click here to download high resolution image

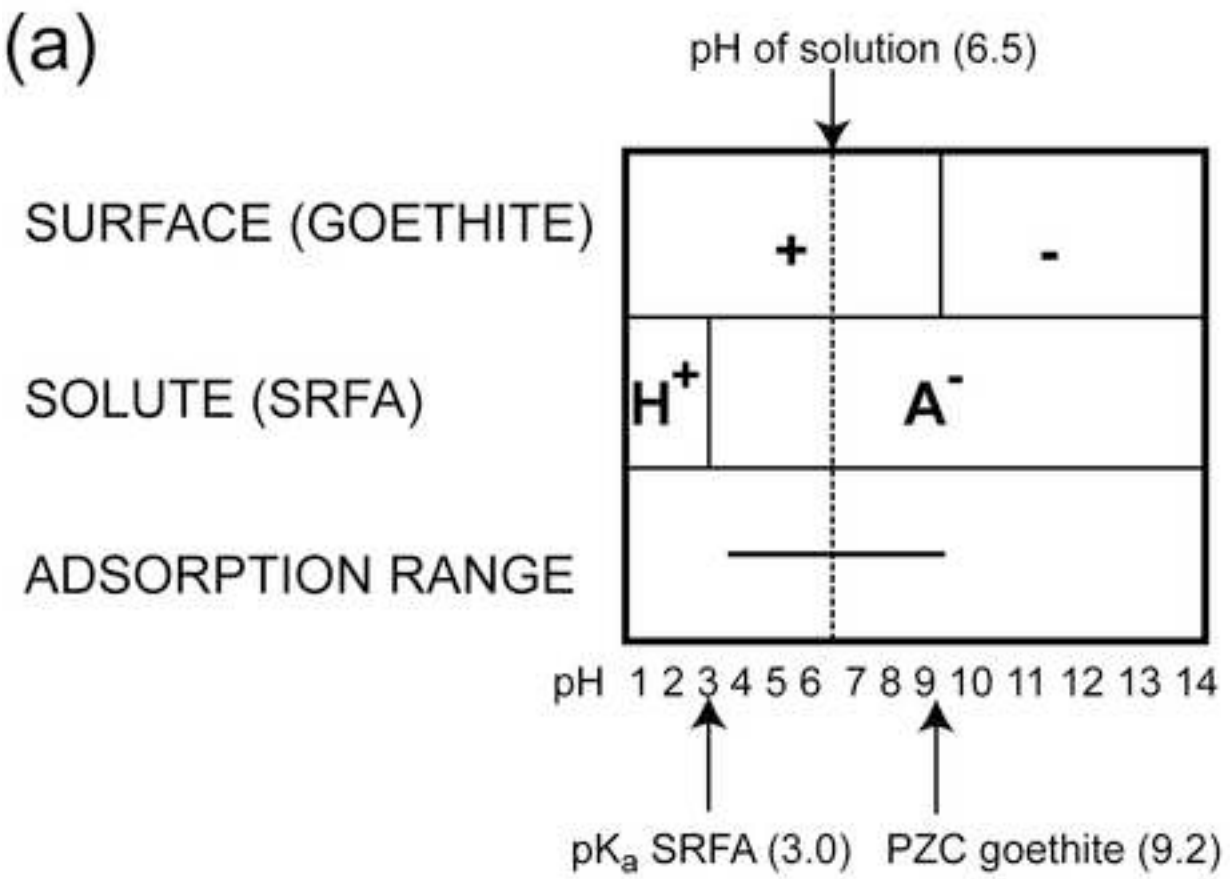

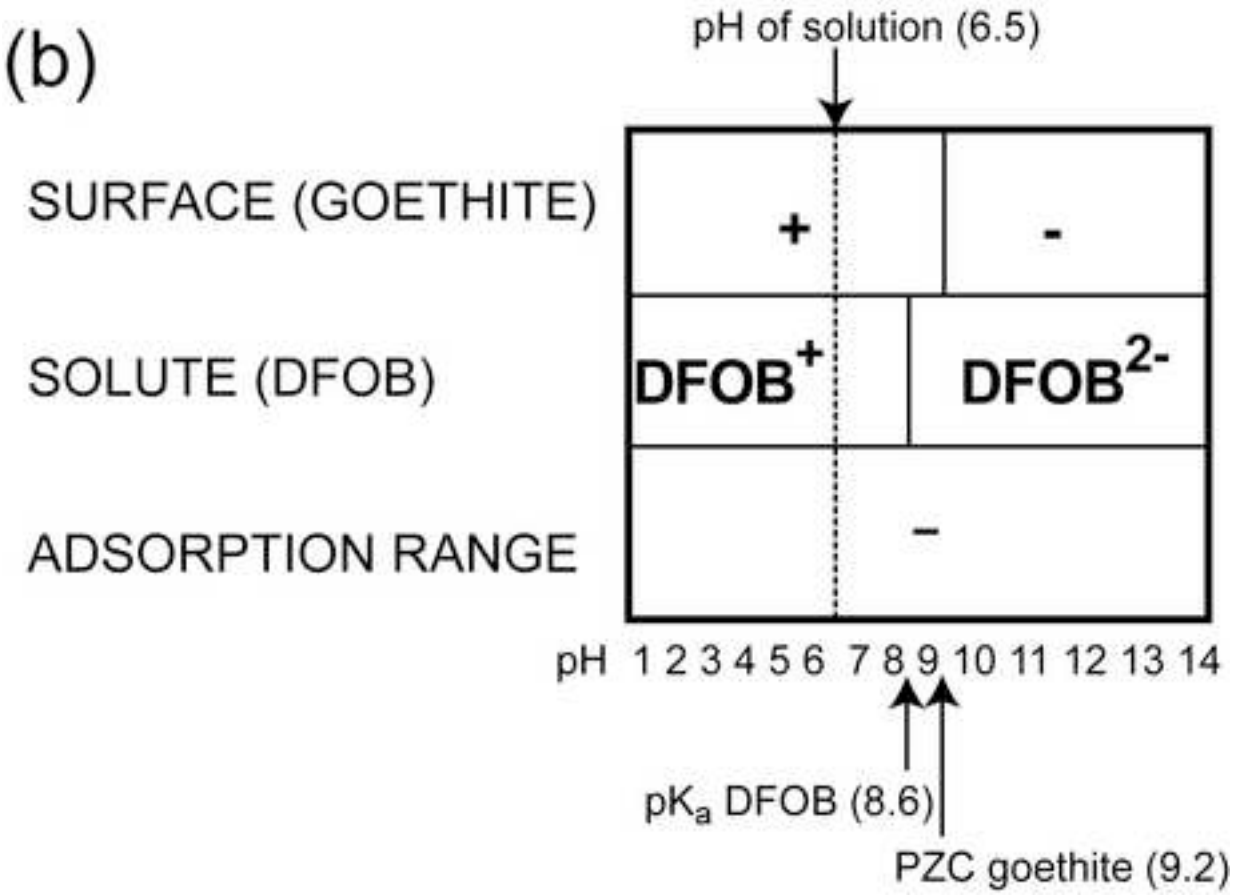

Figure 8

Click here to download high resolution image

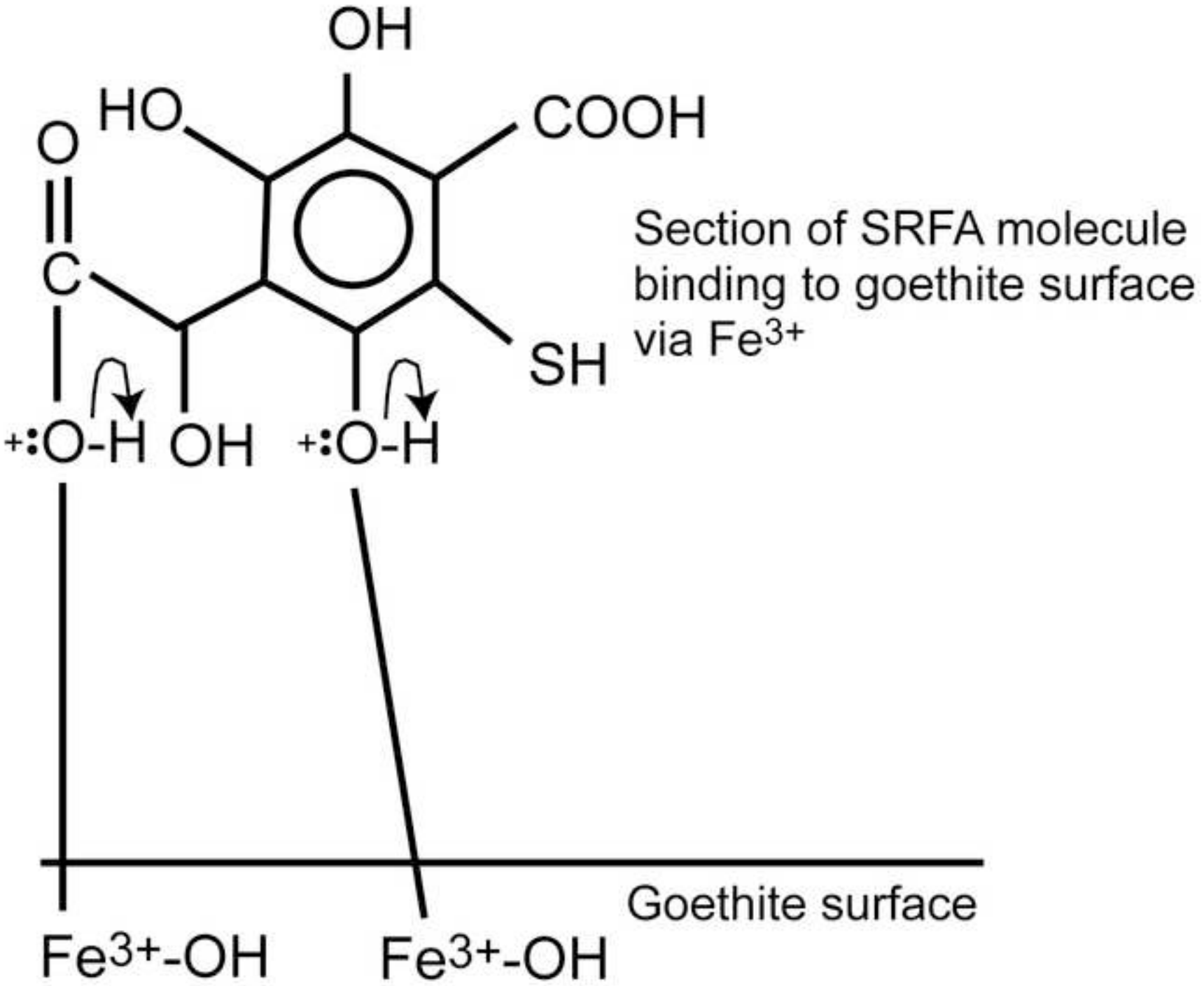

Figure 9

Click here to download high resolution image

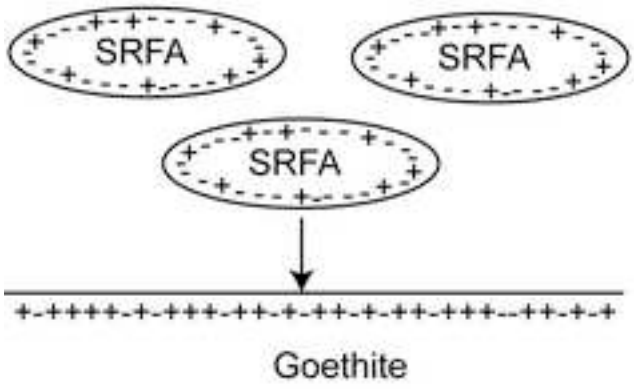

Step 1. At pH 6.5, SRFA surface is negatively charged, and goethite surface is positively charged.

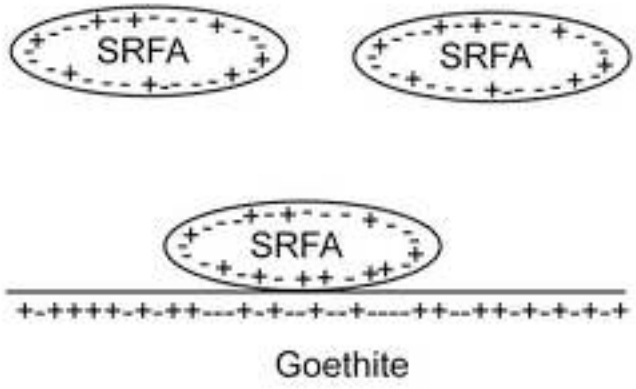

Step 2. Areas on the goethite surface become less positive in the vicinity of the SRFA molecule.

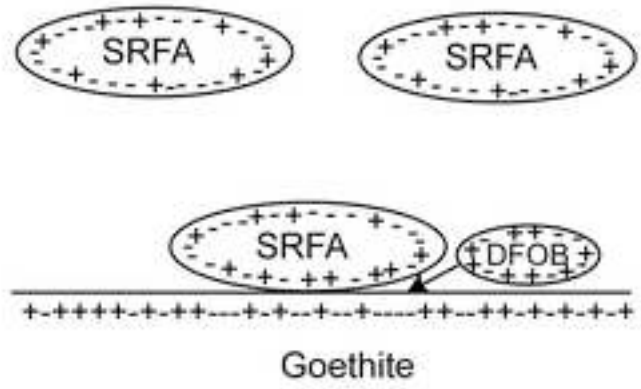

Step 3. The hydroxamate furthest from the protonated amine in the DFOB bonds to the less positive areas on the goethite surface.

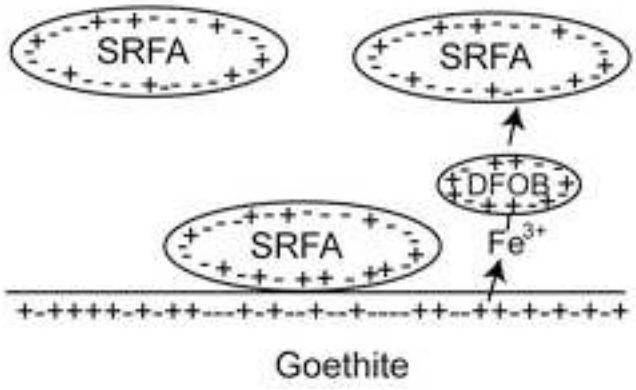

Step 4. DFOB bonds with Fe^{3+} on the goethite surface. The new Fe^{3+}-DFOB complex then detaches from the surface into solution and approaches other SRFA molecules.